

# Exact Force Equilibrium in Linear Elasticity

K. Olesen<sup>1</sup>, B. Gervang<sup>1</sup>, J. N. Reddy<sup>2</sup>, M. Gerritsma<sup>3</sup>

<sup>1</sup>Aarhus University, Department of Engineering, Inge Lehmanns Gade 10, 8000 Aarhus, Denmark, e-mail: keol@eng.au.dk, bge@ase.au.dk.

<sup>2</sup>Department of Mechanical Engineering, Texas A & M University, College Station, TX 77843-3123, USA, e-mail: jnreddy@tamu.edu.

<sup>3</sup>Delft University of Technology, Faculty of Aerospace Engineering, Kluyverweg 2, 2629 HT Delft, The Netherlands, e-mail: m.i.gerritsma@tudelft.nl.

## SUMMARY

In finite element models based on the weak-form Galerkin formulation the equilibrium of forces is satisfied at the computational nodes. In general, however, equilibrium is not satisfied within an element and across inter-element boundaries. Through geometrical considerations of the governing equations, a spectral element method is presented, which satisfies force equilibrium locally as well as globally. The method discretizes displacements at points and forces over surfaces. In this way the force equilibrium equations can be identically satisfied independent of the size or shape of the grid. Since the forces are discretized at surfaces there is a perfect force balance at the boundaries between elements. This also makes the method very robust for even highly deformed meshes, which is illustrated through numerical examples. Copyright © 2016 John Wiley & Sons, Ltd.

Received ...

KEY WORDS: mimetic methods; spectral element method; discrete force equilibrium.

## 1. INTRODUCTION

The finite element method (FEM) is a common tool in the engineering and scientific community to simulate physical problems, and [1, 2, 3, 4] describe the method in depth. The FEM was first developed for structural problems, but later also adapted for heat and fluid problems [5], and now it is applicable for many physical problems such as electromagnetism [6]. In the FEM the unknown quantities of a problem are approximated by polynomial expansions defined in elements of the computational domain. The FEM is based on the differential version of the governing equations, which is defined in *points*, however, the derivation of these equations is based on geometrical observations and these are not represented in the differential equations. In structural problems the consequence is that the governing differential equations of force equilibrium are not satisfied within an element and across inter-element boundaries pointwise [7, p.119]. Newton's third law, which states that an action should have an equal and opposite reaction, is therefore violated at such interfaces. The equations describing structural problems and its variables are very geometrical [8], and a more physically correct approach would be to consider the geometric aspects of the problem, and expand variables associated to geometrical structures such as lines, surfaces and volumes. This will have the following advantages over the traditional FEM:

- The force equilibrium is satisfied locally.
- The method is geometrically robust; it does not break down on highly deformed meshes.

In traditional FEM the stresses are calculated based on the nodal displacement and the best approximation of the stresses are at the Gauss points. This means that stresses must be extrapolated

to boundaries of the element giving a discontinuous stress field across the elements. To make it continuous the values are often averaged, but this can give erroneous results if, for instance, the elements have different material parameters. The approach in this paper expands the stresses based on the forces on the surfaces of the element, and therefore produces continuous stress fields over the element boundaries.

In [9, 10, 11, 12, 13] it was shown that conservation laws can be exactly represented at the discrete level, while the numerical approximation occurs in the constitutive equations. These references consider scalar conservation equations like conservation of mass. In this paper we extend these ideas to vector-valued conservation laws, such as conservation of force equilibrium in continuum mechanics. The method is based on the *mimetic spectral element method* presented in [12, 13, 14], where the variables of the problem are considered as real valued differential  $k$ -forms, which we associate to geometrical objects of dimension  $k$ . The geometry of elastic problems in the discrete setting has been considered in [15], where the elasticity complex was defined. In the work of Yavari, [16], the variables of an elastic problem are represented as *vector- and covector-valued-differential  $k$ -forms*, which means that the variables are associated to geometrical objects of dimension  $k$ , which maps into linear vector spaces. In Yavari's work the constitutive relations expressed in vector-valued exterior calculus are more complicated than the real-valued cases. For further developments of Yavari's work see [17, 18, 19], where the last reference discusses the elastic complex in detail. In the traditional structural FEM there is also a coupling to the geometry, as shown by Reddy and Srinivasa [20], where it was derived that the edges of the elements act like trusses.

The outline of this paper is as follows. In Section 2 the governing equations of a linear elastic problem are given. In Section 3 the geometry of the governing equations is considered and discrete exact versions of the gradient- and divergence-operator are provided. The governing equations based on these geometrical observations are presented in Section 4. In Section 5 the principle of virtual displacements is applied to the equations. The spectral expansion polynomials are presented in Section 6, where also the finite dimensional variational formulation is given. Two test cases are presented in Section 7, while concluding remarks are given in Section 8.

## 2. THE FINITE ELEMENT METHOD

The governing equations for a structural problem in  $\mathbb{R}^3$  are given by the equations of force equilibrium, the strain-displacement relations, and the stress-strain relations, where the latter comprise the constitutive equations. The equations of force equilibrium are given by [4]

$$\mathbf{D}^T \boldsymbol{\sigma} + \mathbf{f} = 0, \quad (1)$$

where  $\boldsymbol{\sigma}$  is a vector of the components of the second order Cauchy stress tensor and  $\mathbf{f}$  is a vector of the body force densities, and  $\mathbf{D}^T$  denotes a matrix differential operators with  $T$  denoting the transpose. In a Cartesian coordinate system we have

$$\mathbf{D}^T = \begin{bmatrix} \frac{\partial}{\partial x_1} & 0 & 0 & \frac{\partial}{\partial x_2} & 0 & \frac{\partial}{\partial x_3} \\ 0 & \frac{\partial}{\partial x_2} & 0 & \frac{\partial}{\partial x_1} & \frac{\partial}{\partial x_3} & 0 \\ 0 & 0 & \frac{\partial}{\partial x_3} & 0 & \frac{\partial}{\partial x_2} & \frac{\partial}{\partial x_1} \end{bmatrix}, \quad \boldsymbol{\sigma} = \begin{Bmatrix} \sigma_{11} \\ \sigma_{22} \\ \sigma_{33} \\ \sigma_{12} \\ \sigma_{23} \\ \sigma_{31} \end{Bmatrix}, \quad \mathbf{f} = \begin{Bmatrix} f_1 \\ f_2 \\ f_3 \end{Bmatrix}, \quad (2)$$

where  $\sigma_{ij} = \sigma_{ji}$ . The strain displacement relations are given by

$$\boldsymbol{\varepsilon} = \mathbf{D} \mathbf{u}, \quad (3)$$

where  $\boldsymbol{\varepsilon}$  contain the components of the second order strain tensor listed in a vector,  $\mathbf{u}$  is the displacement vector and  $\mathbf{D}$  is the gradient matrix, which is the transpose of divergence matrix in

(2), and

$$\boldsymbol{\varepsilon} = \begin{Bmatrix} \varepsilon_{11} \\ \varepsilon_{22} \\ \varepsilon_{33} \\ 2\varepsilon_{12} \\ 2\varepsilon_{23} \\ 2\varepsilon_{31} \end{Bmatrix}, \quad \mathbf{u} = \begin{Bmatrix} u_1 \\ u_2 \\ u_3 \end{Bmatrix}.$$

The constitutive equations can be expressed as

$$\boldsymbol{\sigma} = \mathbf{C}\boldsymbol{\varepsilon}, \quad (4)$$

where  $\mathbf{C}$  is the  $6 \times 6$  matrix of elasticity constants.

For elastic materials the entries of  $\mathbf{C}$  can be expressed in terms of a reduced number of material parameters, elastic moduli and Poisson's ratios or Lamé constants, depending on the material under consideration. The constitutive relation can also be written as

$$\mathbf{C}^{-1}\boldsymbol{\sigma} = \mathbf{D}\mathbf{u}, \quad (5)$$

where  $\mathbf{C}^{-1}$  is the compliance matrix.

Equations (1), (3) and (4) form the starting point of structural finite element expansions [21]. Through the principle of virtual work a variational problem is formulated, the computational domain is divided in a number of elements and the displacement field in each element is expanded typically in Lagrange polynomials. The result is a linear system of algebraic equations among the nodal (and possibly nodless) displacements:

$$\mathbf{K}\boldsymbol{\Delta}_u = \bar{\mathbf{f}},$$

where  $\boldsymbol{\Delta}_u$  is a column vector containing all expansion coefficients for the displacement field,  $\bar{\mathbf{f}}$  contains the expansion coefficients for the force field and  $\mathbf{K}$  is called the *stiffness matrix*.

In this conventional formulation, the governing equations are only satisfied in an integral sense, and locally the equations are only approximately satisfied. For instance, the derivatives in  $\mathbf{D}$  are calculated by differentiating the Lagrange polynomials, which, if  $C^0$  approximations are used in the displacement field, results in discontinuous strain fields between elements and therefore discontinuous stress fields across element boundaries. This is physically not correct since it violates Newton's third law that an action should have an equal and opposite reaction. The stress tensor is defined as the surface force per unit area in the limit for vanishing area [22].

A more physically correct approach would be to treat each element as a free body having forces acting on its boundaries and a body force in the interior. Using surface forces as our degrees of freedom instead of nodal forces and expanding the body forces as volumetric forces will ensure that force equilibrium is satisfied locally.

### 3. A GEOMETRICAL INTERPRETATION OF THE GRADIENT AND DIVERGENCE OPERATOR

The step where we go from an integral model to a differential model is when we take the limits by letting the size of the element approach zero, and thereby obtain the differential versions of the gradient and divergence operators (see [23]). However, these operators (and the curl operator as well, which is not used in this work) are derived based on finite-sized geometrical objects. Therefore, it is possible to evaluate these operators *exactly* in a finite setting, which is the scope of this section.

Starting with the gradient operator, consider the function  $a(x_1, x_2, x_3) \in \mathbb{R}^3$ . The gradient with respect to the coordinate axes  $x_1, x_2$  and  $x_3$  at the point  $p$  describes the local rate of change of scalar function  $a(x_1, x_2, x_3)$  along the coordinate axes at  $p$

$$\text{grad}(a(p)) = \left\langle \left. \frac{\partial a(x_1, x_2, x_3)}{\partial x_1} \right|_p, \left. \frac{\partial a(x_1, x_2, x_3)}{\partial x_2} \right|_p, \left. \frac{\partial a(x_1, x_2, x_3)}{\partial x_3} \right|_p \right\rangle.$$

Taking this back to a finite setting implies integrating between two point, say  $p_1$  and  $p_2$ , along a curve  $\gamma$ , where  $\{p_1, p_2\} = \partial\gamma$ , then by the gradient theorem of calculus [24]

$$\int_{\gamma} \text{grad}(a) = \int_{p_1}^{p_2} \text{grad}(a) = a(p_2) - a(p_1) . \quad (6)$$

The integral of the gradient of a scalar function,  $a$ , is just the difference between the value of  $a$  at the end points of the curve.

The divergence of a vector field

$$\mathbf{q}(x_1, x_2, x_3) = \langle q_1(x_1, x_2, x_3), q_2(x_1, x_2, x_3), q_3(x_1, x_2, x_3) \rangle^T ,$$

in  $\mathbb{R}^3$  in a point  $p$  is given by

$$\text{div}(\mathbf{q}(p)) = \left. \frac{\partial q_1(x_1, x_2, x_3)}{\partial x_1} \right|_p + \left. \frac{\partial q_2(x_1, x_2, x_3)}{\partial x_2} \right|_p + \left. \frac{\partial q_3(x_1, x_2, x_3)}{\partial x_3} \right|_p .$$

Integrating the divergence over a volume,  $\Omega$ , takes it to a finite setting through the divergence theorem [24]

$$\int_{\Omega} \text{div}(\mathbf{q}) = \int_{(\partial\Omega)_1} q_1 dx_2 dx_3 + \int_{(\partial\Omega)_2} q_2 dx_3 dx_1 + \int_{(\partial\Omega)_3} q_3 dx_1 dx_2 , \quad (7)$$

where  $(\partial\Omega)_i$  denotes the area given by the boundary of  $\Omega$  projected to the plane, which the  $i^{\text{th}}$  component of the boundary unit normal vector is normal to. The sign of the integral is positive when the component of the unit normal vector is in the same direction as the  $x_i$ -axis and negative when it is opposite. E.g.  $(\partial\Omega)_1$  will be the boundary projected to the plane spanned by the  $x_2$  and  $x_3$  axes. The divergence operator is seen to be just the sum of all fluxes over the boundary of  $\Omega$  and can easily be calculated. For instance consider a rectangular domain in a Cartesian coordinate system placed as shown in Figure 1 and let

$$Q_i = \int_{(\partial\Omega)_i} q_i dx_1 \cdots \widehat{dx_i} \cdots dx_n , \quad (8)$$

be the fluxes across the boundaries as shown in Figure 1, where  $\widehat{dx_i}$  indicates that this differential is missing, then

$$\int_{\Omega} \text{div}(\mathbf{q}(p)) = (Q_{1,+} - Q_{1,-}) + (Q_{2,+} - Q_{2,-}) + (Q_{3,+} - Q_{3,-}) ,$$

which is exact.

In curvilinear coordinates on complex domains the gradient and divergence can still be easily evaluated. One maps a simple domain, e.g. a square cube in the reference  $(\xi_1, \xi_2, \xi_3)$ -frame to the deformed domain in the  $(x_1, x_2, x_3)$ -frame. Let the coordinates  $x_1, x_2$  and  $x_3$  be functions of the reference coordinates  $\xi_1, \xi_2$  and  $\xi_3$ , hence mapping  $\xi_i \rightarrow x_j(\xi_i)$ , then

$$a(x_1, x_2, x_3) = a(x_1(\xi_1, \xi_2, \xi_3), x_2(\xi_1, \xi_2, \xi_3), x_3(\xi_1, \xi_2, \xi_3)) = a(\xi_1, \xi_2, \xi_3) ,$$

so the integral of the gradient in (6) is the same.

The integral of the divergence is also independent of the coordinate system, which is illustrated in Figure 2, where a square cube,  $\hat{\Omega}$ , in the reference frame is mapped to the deformed domain  $\Omega$  in  $(x_1, x_2, x_3)$ -frame. Performing a change of variables on (7) gives

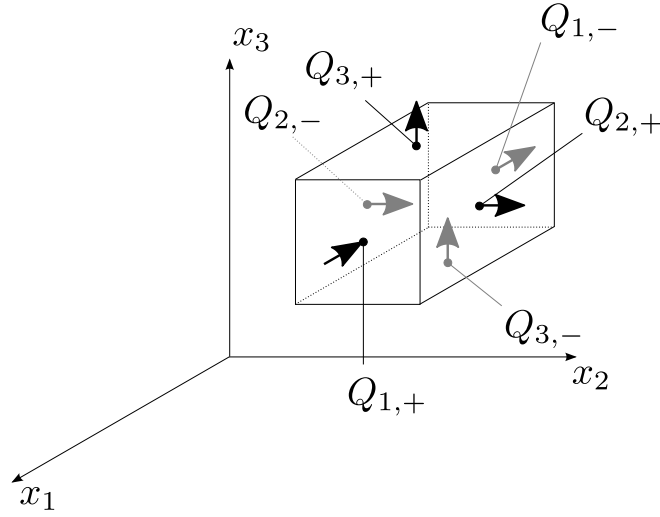


Figure 1. The fluxes across the boundaries of a rectangular domain in a Cartesian coordinate setting.

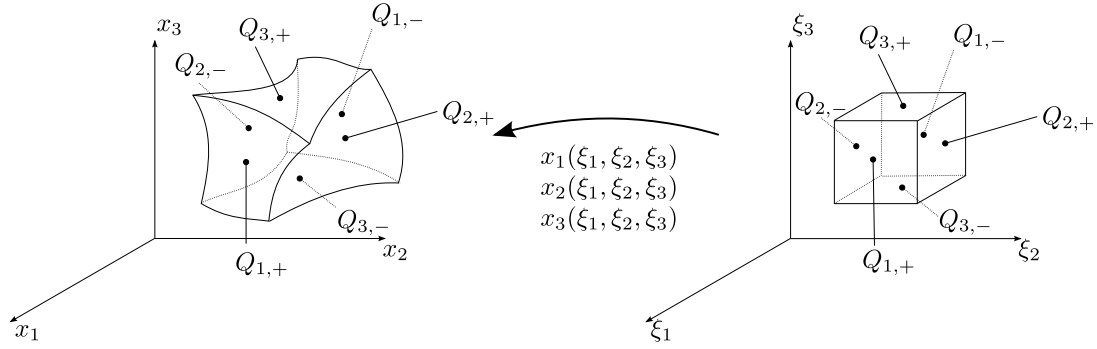


Figure 2. The domain  $\hat{\Omega}$  described in the reference frame  $(\xi_1, \xi_2, \xi_3)$  is mapped to the domain  $\Omega$  in frame  $(x_1, x_2, x_3)$ . The fluxes  $Q_i$  across the boundaries are independent of the frame.

$$\begin{aligned}
 \int_{\Omega} \operatorname{div}(\mathbf{q}) &= \int_{(\partial\hat{\Omega})_1} q_1 \left( \sum_{i=1}^3 \frac{\partial x_2}{\partial \xi_i} d\xi_i \right) \left( \sum_{i=1}^3 \frac{\partial x_3}{\partial \xi_i} d\xi_i \right) \\
 &+ \int_{(\partial\hat{\Omega})_2} q_2(x_1, x_2, x_3) \left( \sum_{i=1}^3 \frac{\partial x_3}{\partial \xi_i} d\xi_i \right) \left( \sum_{i=1}^3 \frac{\partial x_1}{\partial \xi_i} d\xi_i \right) \\
 &+ \int_{(\partial\hat{\Omega})_3} q_3(x_1, x_2, x_3) \left( \sum_{i=1}^3 \frac{\partial x_1}{\partial \xi_i} d\xi_i \right) \left( \sum_{i=1}^3 \frac{\partial x_2}{\partial \xi_i} d\xi_i \right), \quad (9)
 \end{aligned}$$

which can be rearranged to read

$$\begin{aligned}
 \int_{\Omega} \operatorname{div}(\mathbf{q}) &= \int_{(\partial\hat{\Omega})_1} q_1 J_{2323}^{(2)} + q_2 J_{3123}^{(2)} + q_3 J_{1223}^{(2)} d\xi_2 d\xi_3 + \int_{(\partial\hat{\Omega})_2} q_1 J_{2331}^{(2)} + q_2 J_{3131}^{(2)} + q_3 J_{1231}^{(2)} d\xi_3 d\xi_1 \\
 &+ \int_{(\partial\hat{\Omega})_3} q_1 J_{2312}^{(2)} + q_2 J_{3112}^{(2)} + q_3 J_{1212}^{(2)} d\xi_1 d\xi_2, \quad (10)
 \end{aligned}$$

where

$$J_{ijkl}^{(2)} = \frac{\partial x_i}{\partial \xi_k} \frac{\partial x_j}{\partial \xi_l} - \frac{\partial x_i}{\partial \xi_l} \frac{\partial x_j}{\partial \xi_k} . \quad (11)$$

The minus sign comes from the fact that a surface spanned by the unit vectors  $\hat{e}_k$  and  $\hat{e}_l$  in the  $\xi_k$ - and  $\xi_l$ -directions, respectively, has the unit surface normal vector  $\hat{e}_k \times \hat{e}_l = -\hat{e}_l \times \hat{e}_k$ . Equation (10) can be written as

$$\int_{\Omega} \operatorname{div}(\mathbf{q}) = \int_{(\partial\hat{\Omega})_1} \hat{q}_1 d\xi_2 d\xi_3 + \int_{(\partial\hat{\Omega})_2} \hat{q}_2 d\xi_3 d\xi_1 + \int_{(\partial\hat{\Omega})_3} \hat{q}_3 d\xi_1 d\xi_2 , \quad (12)$$

where

$$\begin{aligned} \hat{q}_1 &= q_1 J_{2323}^{(2)} + q_2 J_{3123}^{(2)} + q_3 J_{1223}^{(2)} , \\ \hat{q}_2 &= q_1 J_{2331}^{(2)} + q_2 J_{3131}^{(2)} + q_3 J_{1231}^{(2)} , \\ \hat{q}_3 &= q_1 J_{2312}^{(2)} + q_2 J_{3112}^{(2)} + q_3 J_{1212}^{(2)} . \end{aligned} \quad (13)$$

The fluxes are, however, invariant of the frame and the divergence of the example in Figure 2 is

$$\begin{aligned} \int_{\Omega} \operatorname{div}(\mathbf{q}) &= \int_{(\partial\Omega)_1} q_1 dx_2 dx_3 + \int_{(\partial\Omega)_2} q_2 dx_3 dx_1 + \int_{(\partial\Omega)_3} q_3 dx_1 dx_2 \\ &= \int_{(\partial\hat{\Omega})_1} \hat{q}_1 d\xi_2 d\xi_3 + \int_{(\partial\hat{\Omega})_2} \hat{q}_2 d\xi_3 d\xi_1 + \int_{(\partial\hat{\Omega})_3} \hat{q}_3 d\xi_1 d\xi_2 = \int_{\hat{\Omega}} \operatorname{div}(\hat{\mathbf{q}}) \\ &= (Q_{1,+} - Q_{1,-}) + (Q_{2,+} - Q_{2,-}) + (Q_{3,+} - Q_{3,-}) . \end{aligned} \quad (14)$$

#### 4. GOVERNING EQUATIONS

The governing equations of a structural problem in  $\mathbb{R}^3$  presented in Section 2 are now put in an integral context by applying the constructions presented in Section 3. The computational domain is divided into a number of elements,  $\Omega^s$ . In the following  $i$  denotes an index in the physical domain with coordinates  $(x_1, x_2, x_3)$  and  $\hat{i}$  an index in the reference domain with coordinates  $(\xi_1, \xi_2, \xi_3)$ . The integration of a stress component  $\sigma_{ji}$  over a surface,  $(\partial\Omega)_j$ , produces a surface force component,  $T_{ji}$ , on the surface in direction  $x_i$

$$T_{ji} = \int_{(\partial\Omega)_j} \sigma_{ji} dx_1 \cdots \widehat{dx_j} \cdots dx_n . \quad (15)$$

By comparing this with (8) and (14) then it is evident that the integral of the divergence of the stress tensor over an element is given by

$$\int_{\Omega} \operatorname{div}(\boldsymbol{\sigma}) d\Omega = \left\{ \begin{array}{l} (T_{11,+} - T_{11,-}) + (T_{21,+} - T_{21,-}) + (T_{31,+} - T_{31,-}) \\ (T_{12,+} - T_{12,-}) + (T_{22,+} - T_{22,-}) + (T_{32,+} - T_{32,-}) \\ (T_{13,+} - T_{13,-}) + (T_{23,+} - T_{23,-}) + (T_{33,+} - T_{33,-}) \end{array} \right\} .$$

To account for deformed elements a mapping from the simple domain with coordinates  $(\xi_1, \xi_2, \xi_3)$  to the physical domain with coordinates  $(x_1, x_2, x_3)$  is required. The Cauchy stress tensor must be transformed to the simple domain  $\boldsymbol{\sigma} \rightarrow \hat{\boldsymbol{\sigma}}$ , where  $\hat{\boldsymbol{\sigma}} = [\sigma_{\hat{j}\hat{i}}]$  and  $\hat{j}$  denotes the  $(\xi_1, \xi_2, \xi_3)$ -coordinates and the  $i$  denotes the  $(x_1, x_2, x_3)$ -coordinates. Thus,  $\hat{\boldsymbol{\sigma}}$  denotes the first Piola–Kirchhoff stress tensor (see [30]). If the second index also was transformed then the change of direction of the surface forces should also be accounted for. Put differently, if both indices of the stress tensor are transformed then after integrating over a surface the resulting force component would be normal or tangential to the

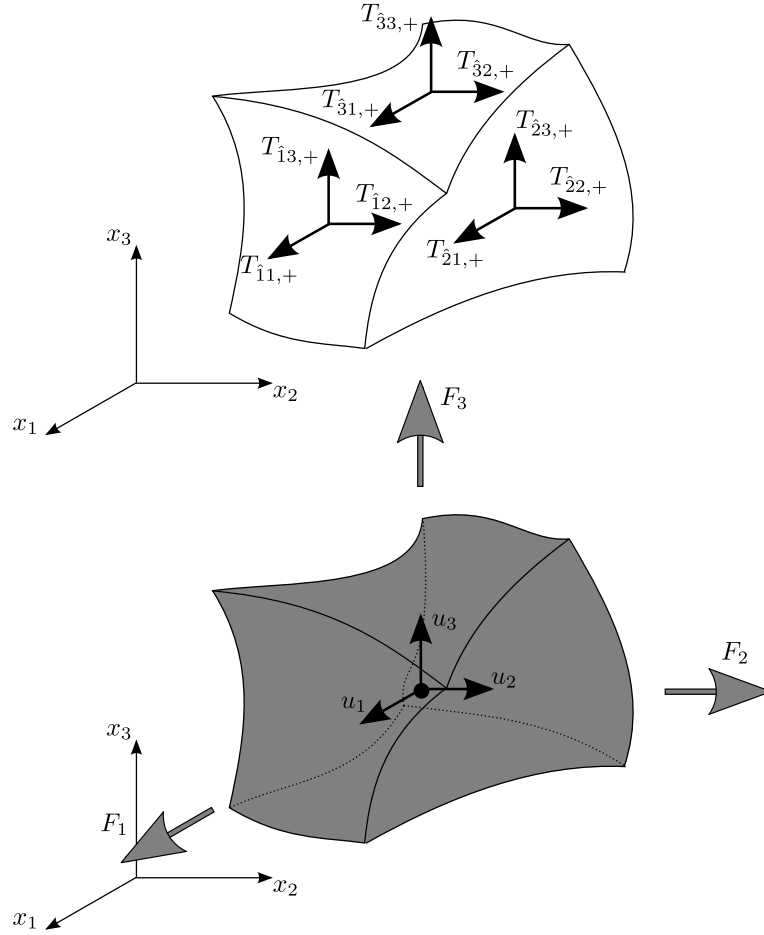


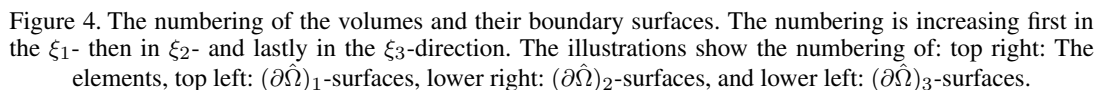
Figure 3. The forces on a element and the displacement in a point inside the element. The top picture illustrates the components of the surface forces on the individual surfaces,  $T_{ij}$ . The bottom picture shows the body force components,  $F_i$ , acting on the volume of the element and the displacement components,  $u_i$ , in a point inside the element.

surface, and a transformation is required to align it with the  $(x_1, x_2, x_3)$ -coordinates. The approach of using the first Piola-Kirchhoff stresses was also considered in [25].

Following the approach from (9) to (14) the surface force component  $T_{ji}$ , which is the result of integrating  $\sigma_{ji}$  over the surface  $(\partial\hat{\Omega})_j$ ,

$$\begin{aligned}
 T_{1i} &= \int_{(\partial\hat{\Omega}^s)_1} \sigma_{1i} J_{2323}^{(2)} + \sigma_{2i} J_{3123}^{(2)} + \sigma_{3i} J_{1223}^{(2)} d\xi_2 d\xi_3 = \int_{(\partial\hat{\Omega}^s)_1} \hat{\sigma}_{1i} d\xi_2 d\xi_3, \\
 T_{2i} &= \int_{(\partial\hat{\Omega}^s)_2} \sigma_{1i} J_{2331}^{(2)} + \sigma_{2i} J_{3131}^{(2)} + \sigma_{3i} J_{1231}^{(2)} d\xi_3 d\xi_1 = \int_{(\partial\hat{\Omega}^s)_2} \hat{\sigma}_{2i} d\xi_3 d\xi_1, \\
 T_{3i} &= \int_{(\partial\hat{\Omega}^s)_3} \sigma_{1i} J_{2312}^{(2)} + \sigma_{2i} J_{3112}^{(2)} + \sigma_{3i} J_{1212}^{(2)} d\xi_1 d\xi_2 = \int_{(\partial\hat{\Omega}^s)_3} \hat{\sigma}_{3i} d\xi_1 d\xi_2. \quad (16)
 \end{aligned}$$

A body force component,  $F_i$ , is acting on the volume of an element, and a displacement component,  $u_i$ , is specified in a point inside the domain as shown on Figure 3. The body force is given by



where  $J$  is the determinant of the Jacobian matrix of the map  $x_i = x_i(\xi_j)$ . The equilibrium of forces can be written as

This relation is purely topological and therefore only depends on how the individual elements are connected. Consider the domain consisting of 8 elements in Figure 4 then the discrete divergence operator is given by the *incidence matrix*  $E_{(3,2)}$ , which is plotted beneath the illustration in Figure 4. The  $(3, 2)$  denotes the connection between the 3D volumes to the 2D surfaces. The row number indicates the volume number and the column number indicates the surface number. A 0 in the matrix indicates that there is no connection between a volume and a surface, a  $-1$  indicates that the outward unit normal of the surface is *opposite* the direction of coordinate basis of the reference domain. A 1 indicates that the outward unit normal of the surface is *in the same* direction as the coordinate basis of the reference domain.

Let  $\Delta_{\hat{r}}$  denote the column vector containing all components of the surface forces arranged as

Let  $N_E$  be the number of elements in the computational domain then the body forces, which typically are known quantities (e.g. the gravity forces), are arranged in the column vector

for  $i = 1, \dots, N_E$ . The equilibrium of forces is then written as

Copyright © 2016 John Wiley & Sons, Ltd.  
Prepared using nmeauth.cls



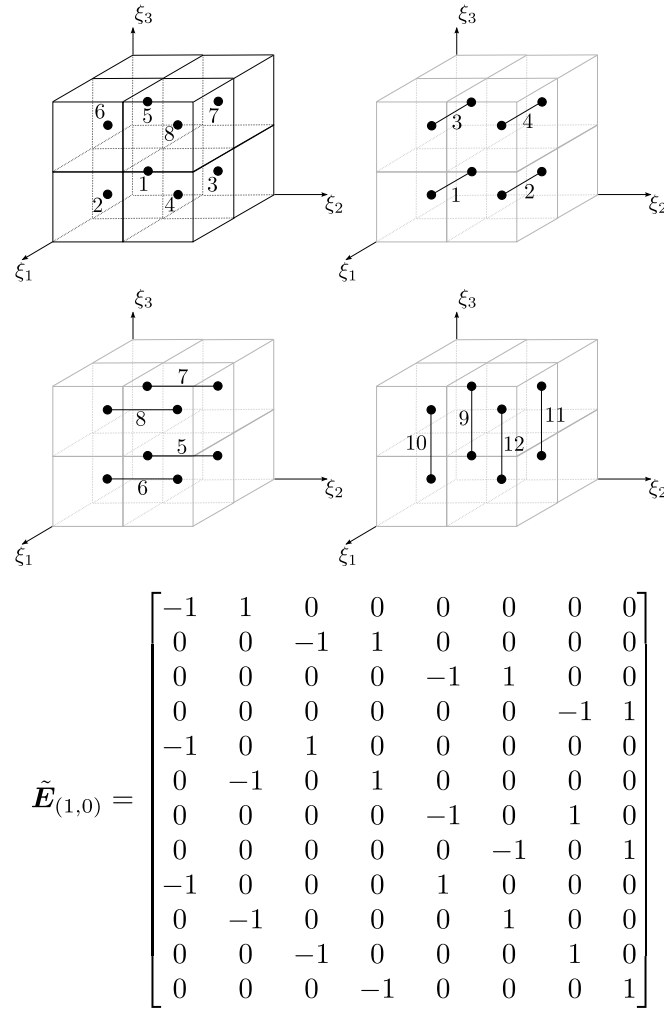


Figure 5. The numbering of the points in the dual grid and the lines they bound. The numbering is increasing first in the  $\xi_1$ - then in  $\xi_2$ - and lastly in the  $\xi_3$ -direction. The illustrations show the numbering of: top right: The points in the dual-grid, top left: The lines on the dual-grid in the  $\xi_1$ -direction, lower right: The lines on the dual-grid in the  $\xi_2$ -direction, and lower The lines on the dual-grid in the  $\xi_3$ -direction.

where

$$\mathcal{D} = \begin{bmatrix} \mathbf{E}_{(3,2)} & 0 & 0 \\ 0 & \mathbf{E}_{(3,2)} & 0 \\ 0 & 0 & \mathbf{E}_{(3,2)} \end{bmatrix}, \quad (21)$$

is the divergence operator. Note that (20) is exact since the degrees of freedom are integral values.

Consider the example of the domain consisting of 8 volumes as in Figure 4 then in each volume a point is chosen and lines are drawn between these points as shown in Figure 5. The grid in Figure 4 and the grid in Figure 5 can be regarded as each other's dual and the grid in Figure 4 is named the *primal grid* and the grid in Figure 5 the *dual grid*, see [9, 12, 26, 27] for the use of dual grids. The connection between the one-dimensional line segments and their boundary points are denoted by the incidence matrix  $\tilde{\mathbf{E}}_{(1,0)}$  plotted beneath the illustration in Figure 5. The *tilde* indicates that it is on the dual grid and (1,0) denotes the connection between the one-dimensional line segments to the zero-dimensional points. The row number indicates the line segment number and the column number indicates the point number. A 0 entry in the matrix  $\tilde{\mathbf{E}}_{(1,0)}$  indicates that there is no connection between a line segment and a point. The lines are oriented such that it coincide with the reference basis. A  $-1$  indicates that this is the point having the lowest  $\xi_i$ -coordinate of the two boundary

points, while a 1 indicates that point has the largest value of the  $\xi_i$ -component of the two boundary points. This is the matrix form of the gradient operator in (6). Let  $\tilde{N}_p$  be the number of points on the dual grid and  $\Delta_u$  denote the column vector of displacements in the points

$$\Delta_u = \{u_1^i \quad u_2^i \quad u_3^i\}^T, \quad (22)$$

for  $i = 1, \dots, \tilde{N}_p$ , where  $\tilde{N}_p = N_E$ , then the gradient operator is given by

$$\mathcal{G} = \begin{bmatrix} \tilde{\mathbf{E}}_{(1,0)} & 0 & 0 \\ 0 & \tilde{\mathbf{E}}_{(1,0)} & 0 \\ 0 & 0 & \tilde{\mathbf{E}}_{(1,0)} \end{bmatrix},$$

and the rate of deformation is found by

$$\Delta_e = \mathcal{G} \Delta_u. \quad (23)$$

If the internal surface force components are isolated, i.e. isolating columns 2, 5, 8, 11, 15, 16, 21, 22, 29, 30, 31 and 32 in  $\mathbf{E}_{(3,2)}$

$$\bar{\mathbf{E}}_{(3,2)} = \begin{bmatrix} 1 & 0 & 0 & 0 & 1 & 0 & 0 & 0 & 1 & 0 & 0 & 0 \\ -1 & 0 & 0 & 0 & 0 & 1 & 0 & 0 & 0 & 1 & 0 & 0 \\ 0 & 1 & 0 & 0 & -1 & 0 & 0 & 0 & 0 & 0 & 1 & 0 \\ 0 & -1 & 0 & 0 & 0 & -1 & 0 & 0 & 0 & 0 & 0 & 1 \\ 0 & 0 & 1 & 0 & 0 & 0 & 1 & 0 & -1 & 0 & 0 & 0 \\ 0 & 0 & -1 & 0 & 0 & 0 & 0 & 1 & 0 & -1 & 0 & 0 \\ 0 & 0 & 0 & 1 & 0 & 0 & -1 & 0 & 0 & 0 & -1 & 0 \\ 0 & 0 & 0 & -1 & 0 & 0 & 0 & -1 & 0 & 0 & 0 & -1 \end{bmatrix},$$

then  $\tilde{\mathbf{E}}_{(1,0)} = -\bar{\mathbf{E}}_{(3,2)}^T$ , and thereby highlights the symmetry between the gradient and the divergence operator. The components of the surface forces are typically prescribed at the boundaries and are therefore not solved for.

Up until now all relations have been expressed in terms of integral relations, however, (5) is equating stresses associated to surfaces with displacement gradients associated to line segments. An interpolation is therefore needed to express the terms on the different geometrical objects, and this is where the numerical approximation is introduced. Equation (5) is stated with respect to the physical domain, so the first Piola-Kirchhoff stress-tensor,  $\hat{\sigma}$ , must be transformed to the Cauchy stress tensor,  $\sigma$ . Consider the surface  $(\partial\hat{\Omega}^s)_i$  in the reference domain and the same surface  $(\partial\Omega^s)_i$  in the spatial domain, then it follows from (15) and (16) that

$$\begin{aligned} T_{ji} &= \int_{(\partial\hat{\Omega})_j} \hat{\sigma}_{ji} d\xi_1 \cdots \widehat{d\xi_j} \cdots d\xi_3 = \int_{(\partial\Omega)_j} \hat{\sigma}_{ji} \left( \sum_{p=1}^3 \frac{\partial \xi_1}{\partial x_p} dx_p \right) \cdots \widehat{d\xi_j} \cdots \left( \sum_{q=1}^3 \frac{\partial \xi_3}{\partial x_q} dx_q \right) \\ &= \int_{(\partial\Omega)_k} \sigma_{ki} dx_1 \cdots \widehat{dx_k} \cdots dx_3. \end{aligned}$$

Gathering the terms then

$$\begin{aligned} \sigma_{1i} &= \hat{\sigma}_{1i} \left( \frac{\partial \xi_2}{\partial x_2} \frac{\partial \xi_3}{\partial x_3} - \frac{\partial \xi_2}{\partial x_3} \frac{\partial \xi_3}{\partial x_2} \right) + \hat{\sigma}_{2i} \left( \frac{\partial \xi_3}{\partial x_2} \frac{\partial \xi_1}{\partial x_3} - \frac{\partial \xi_3}{\partial x_3} \frac{\partial \xi_1}{\partial x_2} \right) + \hat{\sigma}_{2i} \left( \frac{\partial \xi_1}{\partial x_2} \frac{\partial \xi_2}{\partial x_3} - \frac{\partial \xi_1}{\partial x_3} \frac{\partial \xi_2}{\partial x_2} \right), \\ \sigma_{2i} &= \hat{\sigma}_{1i} \left( \frac{\partial \xi_2}{\partial x_3} \frac{\partial \xi_3}{\partial x_1} - \frac{\partial \xi_2}{\partial x_1} \frac{\partial \xi_3}{\partial x_3} \right) + \hat{\sigma}_{2i} \left( \frac{\partial \xi_3}{\partial x_3} \frac{\partial \xi_1}{\partial x_1} - \frac{\partial \xi_3}{\partial x_1} \frac{\partial \xi_1}{\partial x_3} \right) + \hat{\sigma}_{2i} \left( \frac{\partial \xi_1}{\partial x_3} \frac{\partial \xi_2}{\partial x_1} - \frac{\partial \xi_1}{\partial x_1} \frac{\partial \xi_2}{\partial x_3} \right), \\ \sigma_{3i} &= \hat{\sigma}_{1i} \left( \frac{\partial \xi_2}{\partial x_1} \frac{\partial \xi_3}{\partial x_2} - \frac{\partial \xi_2}{\partial x_2} \frac{\partial \xi_3}{\partial x_1} \right) + \hat{\sigma}_{2i} \left( \frac{\partial \xi_3}{\partial x_1} \frac{\partial \xi_1}{\partial x_2} - \frac{\partial \xi_3}{\partial x_2} \frac{\partial \xi_1}{\partial x_1} \right) + \hat{\sigma}_{2i} \left( \frac{\partial \xi_1}{\partial x_1} \frac{\partial \xi_2}{\partial x_2} - \frac{\partial \xi_2}{\partial x_1} \frac{\partial \xi_2}{\partial x_1} \right), \end{aligned}$$

and arranging in a matrix

$$\boldsymbol{\sigma} = \begin{bmatrix} \mathcal{J}^{(2)} & 0 & 0 \\ 0 & \mathcal{J}^{(2)} & 0 \\ 0 & 0 & \mathcal{J}^{(2)} \end{bmatrix} \hat{\boldsymbol{\sigma}} = \boldsymbol{\Phi}_2 \hat{\boldsymbol{\sigma}}, \quad (24)$$

where

$$\mathcal{J}^{(2)} = \begin{bmatrix} (J^{(2)})_{2323}^{-1} & (J^{(2)})_{3123}^{-1} & (J^{(2)})_{1223}^{-1} \\ (J^{(2)})_{2331}^{-1} & (J^{(2)})_{3131}^{-1} & (J^{(2)})_{1231}^{-1} \\ (J^{(2)})_{2312}^{-1} & (J^{(2)})_{3112}^{-1} & (J^{(2)})_{1212}^{-1} \end{bmatrix},$$

with

$$(J^{(2)})_{ijkl}^{-1} = \frac{\partial \xi_i}{\partial x_k} \frac{\partial \xi_j}{\partial x_l} - \frac{\partial \xi_i}{\partial x_l} \frac{\partial \xi_j}{\partial x_k},$$

and  $\boldsymbol{\sigma}$  and  $\hat{\boldsymbol{\sigma}}$  arranged in vectors

$$\begin{aligned} \boldsymbol{\sigma} &= \{\sigma_{11} \quad \sigma_{21} \quad \sigma_{31} \quad \sigma_{12} \quad \sigma_{22} \quad \sigma_{32} \quad \sigma_{13} \quad \sigma_{23} \quad \sigma_{33}\}^T, \\ \hat{\boldsymbol{\sigma}} &= \{\hat{\sigma}_{11} \quad \hat{\sigma}_{21} \quad \hat{\sigma}_{31} \quad \hat{\sigma}_{12} \quad \hat{\sigma}_{22} \quad \hat{\sigma}_{32} \quad \hat{\sigma}_{13} \quad \hat{\sigma}_{23} \quad \hat{\sigma}_{33}\}^T. \end{aligned}$$

Note that  $\boldsymbol{\sigma}$  now has 9 components instead of 6 as in (2). The rate of deformation with respect to  $\xi_j$  is given by

$$\hat{e}_{ji} = \frac{\partial u_i}{\partial \xi_j},$$

so a deformation over a line segment  $\hat{L}$  is described by the vector

$$\left( \int_{\hat{L}} \frac{\partial u_i}{\partial \xi_j} d\xi_j \right) \hat{\boldsymbol{\xi}}_j = \sum_{p=1}^3 \left( \int_{L_p} \frac{\partial u_i}{\partial \xi_j} \left( \frac{\partial \xi_j}{\partial x_p} dx_p \right) \hat{\mathbf{x}}_p \right),$$

where  $\hat{L}$  is the line segment in the reference domain,  $L_p$  is the  $p$ -component of the same line segment in the physical domain and  $\hat{\boldsymbol{\xi}}_j$  and  $\hat{\mathbf{x}}_p$  are the unit vectors in the  $\xi_j$ - and  $x_p$ -directions, respectively. Since the line segment is arbitrary it must hold that

$$\frac{\partial u_i}{\partial \xi_j} \hat{\boldsymbol{\xi}}_j = \sum_{p=1}^3 \left( \frac{\partial u_i}{\partial \xi_j} \frac{\partial \xi_j}{\partial x_p} \hat{\mathbf{x}}_p \right) = \sum_{p=1}^3 \left( \frac{\partial u_i}{\partial x_p} \hat{\mathbf{x}}_p \right),$$

and factoring for  $\hat{\mathbf{x}}_p$  yields

$$\frac{\partial u_i}{\partial x_p} \hat{\mathbf{x}}_p = \sum_{j=1}^3 \left( \frac{\partial u_i}{\partial \xi_j} \frac{\partial \xi_j}{\partial x_p} \hat{\mathbf{x}}_p \right). \quad (25)$$

Remembering that the strains in Cartesian coordinates are given by

$$\varepsilon_{ji} = \frac{1}{2} \left( \frac{\partial u_i}{\partial x_j} + \frac{\partial u_j}{\partial x_i} \right), \quad (26)$$

then by comparing (25) and (26) the relation between strains in the physical frame and the rate of deformation in the reference frame is written by

$$\boldsymbol{\varepsilon} = \boldsymbol{\Phi}_1 \hat{\boldsymbol{\varepsilon}}, \quad (27)$$

where

$$\Phi_1 = \begin{bmatrix} \frac{\partial \xi_1}{\partial x_1} & \frac{\partial \xi_2}{\partial x_1} & \frac{\partial \xi_3}{\partial x_1} & 0 & 0 & 0 & 0 & 0 & 0 \\ \frac{\partial \xi_1}{\partial x_2} & \frac{\partial \xi_2}{\partial x_2} & \frac{\partial \xi_3}{\partial x_2} & \frac{\partial \xi_1}{\partial x_1} & \frac{\partial \xi_2}{\partial x_1} & \frac{\partial \xi_3}{\partial x_1} & 0 & 0 & 0 \\ \frac{\partial \xi_1}{\partial x_3} & \frac{\partial \xi_2}{\partial x_3} & \frac{\partial \xi_3}{\partial x_3} & 0 & 0 & 0 & \frac{\partial \xi_1}{\partial x_1} & \frac{\partial \xi_2}{\partial x_1} & \frac{\partial \xi_3}{\partial x_1} \\ \frac{\partial \xi_1}{\partial x_2} & \frac{\partial \xi_2}{\partial x_2} & \frac{\partial \xi_3}{\partial x_2} & \frac{\partial \xi_1}{\partial x_1} & \frac{\partial \xi_2}{\partial x_1} & \frac{\partial \xi_3}{\partial x_1} & 0 & 0 & 0 \\ 0 & 0 & 0 & \frac{\partial \xi_1}{\partial x_2} & \frac{\partial \xi_2}{\partial x_2} & \frac{\partial \xi_3}{\partial x_2} & 0 & 0 & 0 \\ 0 & 0 & 0 & \frac{\partial \xi_1}{\partial x_3} & \frac{\partial \xi_2}{\partial x_3} & \frac{\partial \xi_3}{\partial x_3} & \frac{\partial \xi_1}{\partial x_2} & \frac{\partial \xi_2}{\partial x_2} & \frac{\partial \xi_3}{\partial x_2} \\ \frac{\partial \xi_1}{\partial x_3} & \frac{\partial \xi_2}{\partial x_3} & \frac{\partial \xi_3}{\partial x_3} & 0 & 0 & 0 & \frac{\partial \xi_1}{\partial x_1} & \frac{\partial \xi_2}{\partial x_1} & \frac{\partial \xi_3}{\partial x_1} \\ 0 & 0 & 0 & \frac{\partial \xi_1}{\partial x_3} & \frac{\partial \xi_2}{\partial x_3} & \frac{\partial \xi_3}{\partial x_3} & \frac{\partial \xi_1}{\partial x_2} & \frac{\partial \xi_2}{\partial x_2} & \frac{\partial \xi_3}{\partial x_2} \\ 0 & 0 & 0 & 0 & 0 & 0 & \frac{\partial \xi_1}{\partial x_3} & \frac{\partial \xi_2}{\partial x_3} & \frac{\partial \xi_3}{\partial x_3} \end{bmatrix}, \quad (28)$$

and

$$\varepsilon = \{\varepsilon_{11} \quad \varepsilon_{21} \quad \varepsilon_{31} \quad \varepsilon_{12} \quad \varepsilon_{22} \quad \varepsilon_{32} \quad \varepsilon_{13} \quad \varepsilon_{23} \quad \varepsilon_{33}\}^T, \\ \hat{e} = \left\{ \frac{\partial u_1}{\partial \xi_1} \quad \frac{\partial u_1}{\partial \xi_2} \quad \frac{\partial u_1}{\partial \xi_3} \quad \frac{\partial u_2}{\partial \xi_1} \quad \frac{\partial u_2}{\partial \xi_2} \quad \frac{\partial u_2}{\partial \xi_3} \quad \frac{\partial u_3}{\partial \xi_1} \quad \frac{\partial u_3}{\partial \xi_2} \quad \frac{\partial u_3}{\partial \xi_3} \right\}^T.$$

The constitutive equation is found by equating (24) and (27)

$$\hat{C}^{-1} \Phi_2 \hat{\sigma} = \Phi_1 \hat{e}, \quad (29)$$

where  $\hat{C}^{-1}$  is the compliance matrix of size  $9 \times 9$  and  $\Phi_2$  is defined in (24). The  $\frac{1}{2}$  in (26) for the shear strains is accounted for in  $\hat{C}^{-1}$ . The symmetry of the Cauchy stress tensor is only weakly enforced through the symmetry of  $\varepsilon$  in (27).

## 5. THE PRINCIPLE OF VIRTUAL WORK

To solve the system it is customary in FEMs to reformulate the problem in a variational statement. The current formulation consists of the equilibrium of forces in (20), the rate of deformation in (23) and the constitutive relation in (29). Multiplying the forces in (20) with the virtual displacement field  $w$  will produce a virtual work. Since (20) is in a finite setting it corresponds to taking the inner product of the virtual displacement vector and the force vectors in (20)

$$(w^h, \text{div}(\hat{\sigma}^h)) = - (w^h, f^h) \\ \Downarrow \\ (\Delta_w, \mathcal{D} \Delta_{\hat{T}}) = - (\Delta_w, F),$$

where

$$\Delta_w = \{w_1^i \quad w_2^i \quad w_3^i\}^T,$$

for  $i = 1, \dots, N_E$ .

To calculate the virtual work of the constitutive equation (29) it is multiplied with the virtual stress field

$$\hat{\varsigma} = \{\varsigma_{11} \quad \varsigma_{21} \quad \varsigma_{31} \quad \varsigma_{12} \quad \varsigma_{22} \quad \varsigma_{32} \quad \varsigma_{13} \quad \varsigma_{23} \quad \varsigma_{33}\}^T,$$

and integrated over the computational domain. However, (29) must be converted to a strain field in the reference frame. This is done by multiplying (29) with  $\Phi_1^{-1}$ , however, looking at (28) it is seen that  $\Phi_1$  is a singular matrix, but this can be circumvented by rewriting (29) as

$$\hat{C}^{-1} \Phi_2 \hat{\sigma} = \Phi_{1,1} \hat{e} + \Phi_{1,2} \hat{e}, \quad (30)$$

where

$$\Phi_{1,1} = \begin{bmatrix} \mathcal{J}^{(1)} & 0 & 0 \\ 0 & \mathcal{J}^{(1)} & 0 \\ 0 & 0 & \mathcal{J}^{(1)} \end{bmatrix}, \quad \text{with} \quad \mathcal{J}^{(1)} = \begin{bmatrix} \frac{\partial \xi_1}{\partial x_1} & \frac{\partial \xi_2}{\partial x_1} & \frac{\partial \xi_3}{\partial x_1} \\ \frac{\partial \xi_1}{\partial x_2} & \frac{\partial \xi_2}{\partial x_2} & \frac{\partial \xi_3}{\partial x_2} \\ \frac{\partial \xi_1}{\partial x_3} & \frac{\partial \xi_2}{\partial x_3} & \frac{\partial \xi_3}{\partial x_3} \end{bmatrix}, \quad (31)$$

and

$$\Phi_{1,2} = \begin{bmatrix} 0 & 0 & 0 & 0 & 0 & 0 & 0 & 0 & 0 \\ 0 & 0 & 0 & \frac{\partial \xi_1}{\partial x_1} & \frac{\partial \xi_2}{\partial x_1} & \frac{\partial \xi_3}{\partial x_1} & 0 & 0 & 0 \\ 0 & 0 & 0 & 0 & 0 & 0 & \frac{\partial \xi_1}{\partial x_1} & \frac{\partial \xi_2}{\partial x_1} & \frac{\partial \xi_3}{\partial x_1} \\ \frac{\partial \xi_1}{\partial x_2} & \frac{\partial \xi_2}{\partial x_2} & \frac{\partial \xi_3}{\partial x_2} & 0 & 0 & 0 & 0 & 0 & 0 \\ 0 & 0 & 0 & 0 & 0 & 0 & 0 & 0 & 0 \\ 0 & 0 & 0 & 0 & 0 & 0 & \frac{\partial \xi_1}{\partial x_2} & \frac{\partial \xi_2}{\partial x_2} & \frac{\partial \xi_3}{\partial x_2} \\ \frac{\partial \xi_1}{\partial x_3} & \frac{\partial \xi_2}{\partial x_3} & \frac{\partial \xi_3}{\partial x_3} & 0 & 0 & 0 & 0 & 0 & 0 \\ 0 & 0 & 0 & \frac{\partial \xi_1}{\partial x_3} & \frac{\partial \xi_2}{\partial x_3} & \frac{\partial \xi_3}{\partial x_3} & 0 & 0 & 0 \\ 0 & 0 & 0 & 0 & 0 & 0 & 0 & 0k & 0 \end{bmatrix}. \quad (32)$$

$\Phi_{1,1}$  is not singular and (30) can be rearranged to

$$\Phi_{1,1}^{-1} \hat{C}^{-1} \Phi_{1,1} \Phi_2 \hat{\sigma} = \hat{e} + \Phi_{1,1}^{-1} \Phi_{1,2} \hat{e}.$$

The virtual work of the constitutive equation is given by

$$\left( \hat{\varsigma}, \Phi_{1,1}^{-1} \hat{C}^{-1} \Phi_{1,1} \Phi_2 \hat{\sigma} \right)_{\hat{\Omega}} - (\hat{\varsigma}, \hat{e})_{\hat{\Omega}} - (\hat{\varsigma}, \Phi_{1,1}^{-1} \Phi_{1,2} \hat{e})_{\hat{\Omega}} = 0,$$

and after integration by parts on the second term

$$\left( \hat{\varsigma}, \Phi_{1,1}^{-1} \hat{C}^{-1} \Phi_{1,1} \Phi_2 \hat{\sigma} \right)_{\hat{\Omega}} + (\text{div}(\hat{\varsigma}), \mathbf{u})_{\hat{\Omega}} - (\hat{\varsigma}, \Phi_{1,1}^{-1} \Phi_{1,2} \hat{e})_{\hat{\Omega}} = (\hat{\varsigma}, \mathbf{u})_{(\partial \hat{\Omega})_u} + (\hat{\varsigma}, \mathbf{u})_{(\partial \hat{\Omega})_T},$$

where  $(\partial \hat{\Omega})_u$  is the part of the boundary, where the displacements are prescribed, and  $(\partial \hat{\Omega})_T$  is the part of the boundary, where the tractions are given.

Let  $\mathcal{V} \subset [H^1(\Omega)]^3$  and  $\mathcal{T} \subset [H_0(\text{div})(\Omega)]^3$  be finite dimensional subspaces, where  $[H^1(\Omega)]^3$  denotes the Sobolev space of vector functions with square-integrable gradients, and  $[H_0(\text{div})(\Omega)]^3$  denotes the Sobolev space of vector functions with square-integrable divergence with vanishing trace along  $(\partial \hat{\Omega})_T$ . The variational statement reads: Find  $(\mathbf{u}^h, \hat{\sigma}^h) \in \mathcal{V} \times \mathcal{T}$  such that:

$$\begin{aligned} (\mathbf{w}^h, \text{div}(\hat{\sigma}^h)) &= -(\mathbf{w}^h, \mathbf{f}^h) \quad \forall \mathbf{w}^h \in \mathcal{V}, \\ \left( \hat{\varsigma}^h, \Phi_{1,1}^{-1} \hat{C}^{-1} \Phi_{1,1} \Phi_2 \hat{\sigma}^h \right)_{\hat{\Omega}} + (\text{div}(\hat{\varsigma}^h), \mathbf{u}^h)_{\hat{\Omega}} - (\hat{\varsigma}^h, \Phi_{1,1}^{-1} \Phi_{1,2} \hat{e}^h)_{\hat{\Omega}} &= (\hat{\varsigma}, \mathbf{u}_{bc})_{(\partial \hat{\Omega})_u} \quad \forall \hat{\varsigma}^h \in \mathcal{T}, \end{aligned} \quad (33)$$

where  $\mathbf{u}_{bc}$  is the known displacements on the  $(\partial \hat{\Omega})_u$  boundary.

## 6. SPECTRAL ELEMENT BASIS FUNCTIONS

This section describes the expansion polynomials applied to the unknowns. Traditionally in FEM the unknowns are expanded based on point values using Lagrange polynomials. Here there is a need to expand quantities based on integrated values. These kind of interpolations are known as histopolations, and in [14] polynomial functions are derived having similar properties as Lagrange polynomials, but in an integral sense. These polynomials are called *edge polynomials*, and they are derived from Lagrange polynomials. Consider the nodal points,  $\xi_i$ ,  $i = 0, \dots, N$ , then the Lagrange

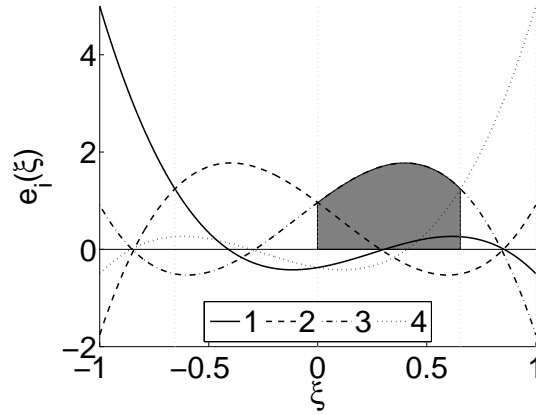


Figure 6. Edge polynomials associated to the Gauss-Lobatto-Legendre points of polynomial degree four. The property  $\int_{\xi_{k-1}}^{\xi_k} e_i(\xi) d\xi = \delta_{i,k}$  is highlighted for the  $e_2(\xi)$  polynomial.

polynomial can be written as:

$$h_i(\xi) = \frac{\prod_{j=0, j \neq i}^N (\xi - \xi_j)}{\prod_{j=0, j \neq i}^N (\xi_i - \xi_j)},$$

which has the properties:

$$\sum_{i=0}^N h_i(\xi) = 1, \quad h_i(\xi_j) = \delta_{i,j}.$$

The polynomial edge functions are related to the Lagrange polynomials by, [14]:

$$e_i(\xi) = - \sum_{k=0}^{i-1} \frac{dh_k(\xi)}{d\xi} =, \quad i = 1, \dots, N,$$

which gives the property:

$$\int_{\xi_{k-1}}^{\xi_k} e_i(\xi) d\xi = \delta_{i,k} = \begin{cases} 1 & \text{if } i = k \\ 0 & \text{if } i \neq k \end{cases},$$

and is illustrated in Figure 6.

Let  $\xi_i, i = 0, \dots, N$  be the Gauss-Lobatto-Legendre (GLL) points of polynomial degree  $N$  and  $\tilde{\xi}_i, i = 1, \dots, N$  the Gauss-Legendre (GL) points. Note that  $\xi_{i-1} < \tilde{\xi}_i < \xi_i$ , for  $i = 1, \dots, N$ . The Lagrange polynomials associated with the GLL points will be denoted by  $h_i(\xi)$  and the Lagrange polynomials associated with the GL points will be denoted by  $\tilde{h}_i(\xi)$ . For more details see [28]. The edge polynomial  $e_i(\xi)$  is a polynomial of degree  $N - 1$  and  $\tilde{e}_i(\xi)$  is a polynomial of degree  $N - 2$ . The  $m$  component of the displacement on the dual grid are in each element expanded as

$$u_m^h(\xi_1, \xi_2, \xi_3) = \sum_{i=0}^{N-1} \sum_{j=0}^{N-1} \sum_{k=0}^{N-1} (u_m)_{i,j,k} \tilde{h}_i(\xi_1) \tilde{h}_j(\xi_2) \tilde{h}_k(\xi_3), \quad (34)$$

This is expressed in vector-form as

$$\mathbf{u}^h = \begin{bmatrix} \tilde{\Psi}^{(0)} & 0 & 0 \\ 0 & \tilde{\Psi}^{(0)} & 0 \\ 0 & 0 & \tilde{\Psi}^{(0)} \end{bmatrix} \Delta_u = \tilde{\mathcal{I}}^{(0)} \Delta_u,$$

where  $\tilde{\Psi}^{(0)}$  is a matrix with the Lagrange polynomials of (34), where the rows denote the evaluation points and the column denotes the discrete displacements of  $\Delta_u$ . Let the gradient of

the displacement component  $m$ ,  $\frac{\partial u_m}{\partial \xi_i}$ , be denoted by  $\partial_i u_m$ . Then the displacement gradients on the dual grid are expanded by

$$\partial_1 u_m^h(\xi_1, \xi_2, \xi_3) = \sum_{i=1}^{N-1} \sum_{j=0}^{N-1} \sum_{k=0}^{N-1} \left( \int_{\hat{L}_1} \partial_1 u_m \right)_{i,j,k} \tilde{e}_i(\xi_1) \tilde{h}_j(\xi_2) \tilde{h}_k(\xi_3), \quad (35)$$

$$\partial_2 u_m^h(\xi_1, \xi_2, \xi_3) = \sum_{i=0}^{N-1} \sum_{j=1}^{N-1} \sum_{k=0}^{N-1} \left( \int_{\hat{L}_2} \partial_2 u_m \right)_{i,j,k} \tilde{h}_i(\xi_1) \tilde{e}_j(\xi_2) \tilde{h}_k(\xi_3), \quad (36)$$

$$\partial_3 u_m^h(\xi_1, \xi_2, \xi_3) = \sum_{i=0}^{N-1} \sum_{j=0}^{N-1} \sum_{k=1}^{N-1} \left( \int_{\hat{L}_3} \partial_3 u_m \right)_{i,j,k} \tilde{h}_i(\xi_1) \tilde{h}_j(\xi_2) \tilde{e}_k(\xi_3), \quad (37)$$

and in vector-form this is expressed as

$$\hat{e}^h = \begin{bmatrix} \tilde{\Psi}^{(1)} & 0 & 0 \\ 0 & \tilde{\Psi}^{(1)} & 0 \\ 0 & 0 & \tilde{\Psi}^{(1)} \end{bmatrix} \mathcal{G} \Delta_u = \tilde{\mathcal{I}}^{(1)} \mathcal{G} \Delta_u, \quad \text{with} \quad \tilde{\Psi}^{(1)} = \begin{bmatrix} \tilde{\Psi}_1^{(1)} & 0 & 0 \\ 0 & \tilde{\Psi}_2^{(1)} & 0 \\ 0 & 0 & \tilde{\Psi}_3^{(1)} \end{bmatrix},$$

where the integrals in (35)-(37) are given by  $\mathcal{G} \Delta_u$ .  $\tilde{\Psi}_i^{(1)}$  are matrices containing the expansion polynomials for (35), (36) and (37), respectively, where the rows denote the evaluation points and the column denotes the discrete values of  $\mathcal{G} \Delta_u$ . The stresses on the primal grid are expanded by

$$\sigma_{1m}^h(\xi_1, \xi_2, \xi_3) = \sum_{i=0}^N \sum_{j=1}^N \sum_{k=1}^N (T_{1m})_{i,j,k} h_i(\xi_1) e_j(\xi_2) e_k(\xi_3), \quad (38)$$

$$\sigma_{2m}^h(\xi_1, \xi_2, \xi_3) = \sum_{i=1}^N \sum_{j=0}^N \sum_{k=1}^N (T_{2m})_{i,j,k} e_i(\xi_1) h_j(\xi_2) e_k(\xi_3), \quad (39)$$

$$\sigma_{3m}^h(\xi_1, \xi_2, \xi_3) = \sum_{i=1}^N \sum_{j=1}^N \sum_{k=0}^N (T_{3m})_{i,j,k} e_i(\xi_1) e_j(\xi_2) h_k(\xi_3), \quad (40)$$

and in vector-form this is expressed as

$$\hat{\sigma}^h = \begin{bmatrix} \Psi^{(2)} & 0 & 0 \\ 0 & \Psi^{(2)} & 0 \\ 0 & 0 & \Psi^{(2)} \end{bmatrix} \Delta_{\hat{T}} = \mathcal{I}^{(2)} \Delta_{\hat{T}}, \quad \text{with} \quad \Psi^{(2)} = \begin{bmatrix} \Psi_1^{(2)} & 0 & 0 \\ 0 & \Psi_2^{(2)} & 0 \\ 0 & 0 & \Psi_3^{(2)} \end{bmatrix}.$$

Here  $\Psi_i^{(2)}$  are matrices containing the expansion polynomials for (38), (39) and (40), respectively, where the rows denote the evaluation points and the column denotes the discrete values of  $\Delta_{\hat{T}}$ . The last expansion is for the body force component  $m$  on the primal grid

$$\hat{f}_m^h = \sum_{i=1}^N \sum_{j=1}^N \sum_{k=1}^N (F_m)_{i,j,k} e_i(\xi_1) e_j(\xi_2) e_k(\xi_3), \quad (41)$$

and in vector-form

$$\hat{f}^h = \begin{bmatrix} \Psi^{(3)} & 0 & 0 \\ 0 & \Psi^{(3)} & 0 \\ 0 & 0 & \Psi^{(3)} \end{bmatrix} \mathbf{F} = \mathcal{I}^{(3)} \mathbf{F}, \quad (42)$$

where the vector of  $\mathbf{F}$  is defined in (19).  $\Psi^{(3)}$  is a matrix with the expansion polynomials of (41), where the rows denote the evaluation points and the column denotes the discrete values of  $\mathbf{F}$ . Within each element there are volumes generated by the GLL grid, and these are referred to as *interior*

elements. Each interior element has a body force and displacement associated to it and it is bounded by surface forces.

Let  $\Delta_{\hat{S}}$  contain all the expansion coefficients for  $\hat{\zeta}_{ji}$

$$\Delta_{\hat{S}} = \{S_{11}^i \quad S_{21}^i \quad S_{31}^i \quad S_{12}^i \quad S_{22}^i \quad S_{32}^i \quad S_{13}^i \quad S_{23}^i \quad S_{33}^i\}^T,$$

with

$$S_{ji} = \int_{(\partial\hat{\Omega})_j} \hat{\zeta}_{ji} d\xi_1 \cdots d\widehat{\xi_j} \cdots d\xi_n,$$

then the variational statement (33) can now be expressed in matrix form as

$$(\Delta_w)^T \Delta_{\hat{T}} = -(\Delta_w)^T \mathbf{F} \quad \forall \Delta_w, \quad (43)$$

$$\begin{aligned} (\Delta_{\hat{S}})^T \sum_{s=1}^{N_E} \left( \int_{\hat{\Omega}^s} (\mathcal{I}^{(2)})^T \Phi_{1,1}^{-1} \hat{C}^{-1} \Phi_2 \mathcal{I}^{(2)} d\Omega^s \right) \Delta_{\hat{T}} \\ + (\Delta_{\hat{S}})^T \mathcal{D}^T \sum_{s=1}^{N_E} \left( \int_{\hat{\Omega}^s} (\mathcal{I}^{(3)})^T \tilde{\mathcal{I}}^{(0)} d\Omega^s \right) \Delta_u \\ - (\Delta_{\hat{S}})^T \sum_{s=1}^{N_E} \left( \int_{\hat{\Omega}^s} (\mathcal{I}^{(2)})^T (\Phi_{1,1})^{-1} \Phi_{1,2} \tilde{\mathcal{I}}^{(1)} d\Omega^s \right) \mathcal{G} \Delta_u \\ = \int_{(\partial\hat{\Omega})_u} (\Delta_{\hat{S}})^T (\mathcal{I}^{(2)})^T \mathbf{u}_{bc} d(\partial\hat{\Omega})_u \quad \forall \Delta_S. \quad (44) \end{aligned}$$

The operators  $\mathcal{D}$  and  $\mathcal{G}$  are global operators.  $\mathcal{D}$  maps physical quantities on surfaces to volumes, and hence must be expanded by  $\mathcal{I}^{(3)}$  defined in (42). The second term and the right hand side in (44) are integrated using a GL quadrature rule while the first and third term are integrated with a GLL quadrature. In (43) and (44) it is assumed that  $\mathbf{F}$  and  $\mathbf{u}_{bc}$  on  $(\partial\hat{\Omega})_u$  are known. However, often it is the body force densities that are known, so they must be integrated over the individual elements to produce  $\mathbf{F}$ . It is rather straightforward to use the expansion polynomials instead. Let  $f_i(x_1, x_2, x_3)$  be the known  $i^{\text{th}}$  component of the body force density, then from (17) and (41) it is clear that

$$J f_i^s(x_1, x_2, x_3) = \hat{f}_i^s(\xi_1, \xi_2, \xi_3) = \Psi^{(3)}(\xi_1, \xi_2, \xi_3) \mathbf{F}_i,$$

where  $\mathbf{F}_i$  is the part of the vector  $\mathbf{F}$  containing the discrete values of the  $i^{\text{th}}$  component of the body forces, and  $J$  is the determinant of the Jacobian matrix. By evaluating this expression in one point in each interior domain, e.g. in the GL points, a square linear system of equations can be set up

$$\Psi_{\xi_{GL}}^{(3)} \hat{\mathbf{F}}_i^s = (J f_{x_i}^s)_{\xi_{GL}} \Rightarrow \hat{\mathbf{F}}_i^s = \left( \Psi_{\xi_{GL}}^{(3)} \right)^{-1} (J f_{x_i}^s)_{\xi_{GL}}.$$

On the  $(\partial\hat{\Omega})_T$ -boundary the forces are specified and since discrete force values are located on the surfaces they can be implemented strongly. However, typically the tractions normal and tangential to a surface are known. Therefore, they must be converted to forces in the reference frame. Consider the three known orthogonal traction components on the surface in  $\mathbb{R}^3$  shown on Figure 7. The  $\sigma_n$  component is in the direction of the unit surface normal vector

$$\mathbf{n} = \{n_1 \quad n_2 \quad n_3\}^T,$$



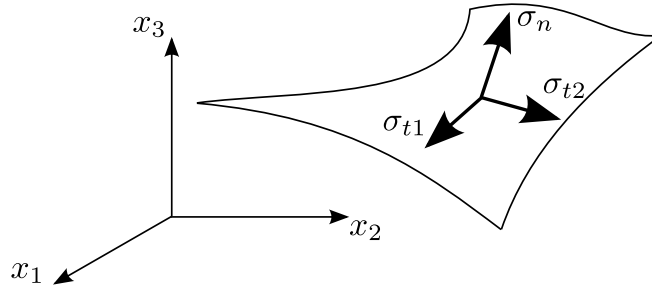


Figure 7. The tractions on a surface in  $\mathbb{R}^3$ . The tractions have three orthogonal components;  $\sigma_n$  in the direction of the unit surface normal vector  $\mathbf{n}$ , and  $\sigma_{t1}$  and  $\sigma_{t2}$  in the directions of the unit surface tangential vectors  $\mathbf{t}_1$  and  $\mathbf{t}_2$ , respectively.

and the components  $\sigma_{t1}$  and  $\sigma_{t2}$  are in the directions of the unit surface tangential vectors

$$\mathbf{t}_1 = \{(t_1)_1 \ (t_1)_2 \ (t_1)_3\}^T, \quad \text{and} \quad \mathbf{t}_2 = \{(t_2)_1 \ (t_2)_2 \ (t_2)_3\}^T,$$

respectively. The traction components in the physical directions are given by

$$\begin{Bmatrix} \sigma_1 \\ \sigma_2 \\ \sigma_3 \end{Bmatrix} = [\mathbf{n} \ \mathbf{t}_1 \ \mathbf{t}_2] \begin{Bmatrix} \sigma_n \\ \sigma_{t1} \\ \sigma_{t2} \end{Bmatrix}.$$

Let the expansion of a boundary of an element be given by

$$\sigma_{\hat{n}m}^{b,h} = \sum_{i=1}^N \sum_{j=1}^N (T_{\hat{n}m})_{i,j} e_i((\xi_b)_1) e_j((\xi_b)_2) = \Psi^{(2),b} \Delta_{\hat{T}}^b,$$

where  $(\xi_b)_i$  denotes the reference coordinates on the boundary and  $\Delta_{\hat{T}}^b$  are the force components in  $\Delta_{\hat{T}}$  that lie on the boundary. Using (10) to (12) then

$$\begin{Bmatrix} \sigma_1 J_{2323}^{(2)} + \sigma_2 J_{3123}^{(2)} + \sigma_3 J_{1223}^{(2)} \\ \sigma_1 J_{2331}^{(2)} + \sigma_2 J_{3131}^{(2)} + \sigma_3 J_{1231}^{(2)} \\ \sigma_1 J_{2312}^{(2)} + \sigma_2 J_{3112}^{(2)} + \sigma_3 J_{1212}^{(2)} \end{Bmatrix} = \begin{bmatrix} \Psi^{(2),b} & 0 & 0 \\ 0 & \Psi^{(2),b} & 0 \\ 0 & 0 & \Psi^{(2),b} \end{bmatrix} \Delta_{\hat{T}}^b,$$

where  $J_{ijkl}^{(2)}$  is specified by (11). By evaluating in the GL points a square linear equation system is produced and solved

$$\Delta_{\hat{T}}^b = \begin{bmatrix} \Psi_{\xi_{GL}}^{(2),b} & 0 & 0 \\ 0 & \Psi_{\xi_{GL}}^{(2),b} & 0 \\ 0 & 0 & \Psi_{\xi_{GL}}^{(2),b} \end{bmatrix}^{-1} \begin{Bmatrix} \left( \sigma_1 J_{2323}^{(2)} + \sigma_2 J_{3123}^{(2)} + \sigma_3 J_{1223}^{(2)} \right) \xi_{GL} \\ \left( \sigma_1 J_{2331}^{(2)} + \sigma_2 J_{3131}^{(2)} + \sigma_3 J_{1231}^{(2)} \right) \xi_{GL} \\ \left( \sigma_1 J_{2312}^{(2)} + \sigma_2 J_{3112}^{(2)} + \sigma_3 J_{1212}^{(2)} \right) \xi_{GL} \end{Bmatrix}.$$

These forces can be implemented strongly in the equation system.

## 7. NUMERICAL RESULTS

Some numerical test cases are now presented. The test cases are in 2D and Hooke's generalized law is the constitutive relation with the assumption of plain stress. This means that the compliance

matrix in (29) is reduced to

$$\hat{C}^{-1} = \frac{1}{E} \begin{bmatrix} 1 & 0 & 0 & -\nu \\ 0 & 2(1+\nu) & 0 & 0 \\ 0 & 0 & 2(1+\nu) & 0 \\ -\nu & 0 & 0 & 1 \end{bmatrix}, \quad (45)$$

where  $E$  is Young's modulus, which is set to  $E = 1$ , and  $\nu$  is Poisson's ratio, which is set to  $\nu = 0.3$ . The matrices  $\Phi_2$  and  $\Phi_{1,i}$  in (24), (31) and (32) then reduce to

$$\Phi_2 = \begin{bmatrix} \frac{\partial \xi_2}{\partial x_2} & -\frac{\partial \xi_1}{\partial x_2} & 0 & 0 \\ -\frac{\partial \xi_2}{\partial x_1} & \frac{\partial \xi_1}{\partial x_1} & 0 & 0 \\ 0 & 0 & \frac{\partial \xi_2}{\partial x_2} & -\frac{\partial \xi_1}{\partial x_2} \\ 0 & 0 & -\frac{\partial \xi_2}{\partial x_1} & \frac{\partial \xi_1}{\partial x_1} \end{bmatrix},$$

and

$$\Phi_{1,1} = \begin{bmatrix} \frac{\partial \xi_1}{\partial x_1} & \frac{\partial \xi_2}{\partial x_1} & 0 & 0 \\ \frac{\partial \xi_1}{\partial x_2} & \frac{\partial \xi_2}{\partial x_2} & 0 & 0 \\ 0 & 0 & \frac{\partial \xi_1}{\partial x_1} & \frac{\partial \xi_2}{\partial x_1} \\ 0 & 0 & \frac{\partial \xi_1}{\partial x_2} & \frac{\partial \xi_2}{\partial x_2} \end{bmatrix}, \quad \Phi_{1,2} = \begin{bmatrix} 0 & 0 & 0 & 0 \\ 0 & 0 & \frac{\partial \xi_1}{\partial x_1} & \frac{\partial \xi_2}{\partial x_1} \\ \frac{\partial \xi_1}{\partial x_2} & \frac{\partial \xi_2}{\partial x_2} & 0 & 0 \\ 0 & 0 & 0 & 0 \end{bmatrix}.$$

### 7.1. Verification Case

First the rate of convergence and the robustness of the method is demonstrated by solving the manufactured solution given by

$$\begin{aligned} u_1(x_1, x_2) &= \sin(2\pi x_1) \cos(2\pi x_2), \\ u_2(x_1, x_2) &= \cos(2\pi x_1) \sin(2\pi x_2), \\ \sigma_{11}(x_1, x_2) &= \sigma_{22}(x_1, x_2) = \frac{\cos(2\pi x_1) \cos(2\pi x_2) 2E\pi}{1-\nu}, \\ \sigma_{12}(x_1, x_2) &= -\frac{\sin(2\pi x_1) \sin(2\pi x_2) 2E\pi}{1+\nu}, \\ f_1(x_1, x_2) &= -\frac{\sin(2\pi x_1) \cos(2\pi x_2) 8E\pi^2}{1-\nu^2}, \\ f_2(x_1, x_2) &= -\frac{\cos(2\pi x_1) \sin(2\pi x_2) 8E\pi^2}{1-\nu^2}, \end{aligned}$$

on the domain  $\Omega \in [-1, 1]^2$  with the mapping

$$\begin{aligned} x_1(\xi_1, \xi_2) &= \xi_1 + c \sin(\pi \xi_1) \sin(\pi \xi_2), \\ x_2(\xi_1, \xi_2) &= \xi_2 + c \sin(\pi \xi_1) \sin(\pi \xi_2), \end{aligned}$$

which is shown in Figure 8 for  $c = \{0, 0.15, 0.3\}$ . The boundary conditions are the exact displacements on all boundaries implemented weakly through  $\int_{(\partial\hat{\Omega})_u} (\Delta_{\hat{S}})^T (\mathcal{I}^{(2)})^T \mathbf{u}_{bc} d(\partial\hat{\Omega})_u$

in (44). A convergence study is performed for the polynomials  $N = \{2, 5, 10\}$ . The convergence in the infinity norm

$$|z|_{\infty} = \max(|z_1|, \dots, |z_n|), \quad (46)$$

for  $z = \{z_1, \dots, z_n\}^T$ , is drawn in a logarithmic scale with respect to the undeformed size of the element,  $h_{el}$ . In (46)  $z$  denotes the expansion of the unknown variables in a preselected amount of points, e.g.  $z_i = u_m^h(\xi_{1,i}, \xi_{2,i}, \xi_{3,i})$  from (34). Convergence of the displacement field is presented in Figure 9, convergence of the normal stress field is presented in Figure 10 and convergence of the

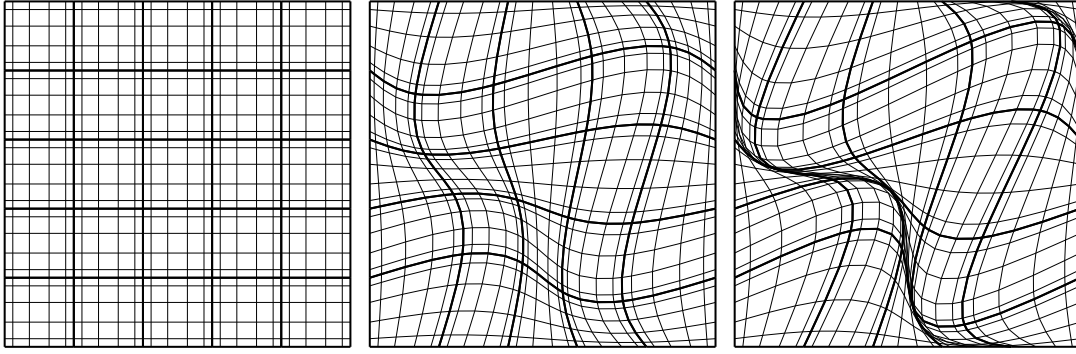


Figure 8. Deformed grids for  $5 \times 5$  elements with  $N = 5$  and  $c = \{0, 0.15, 0.3\}$ .

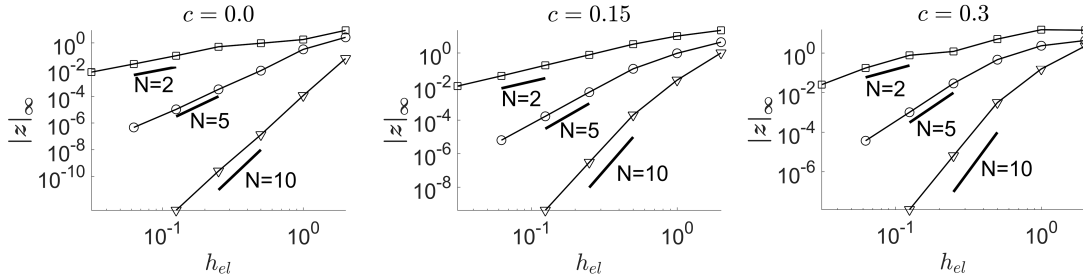


Figure 9. Convergence for  $u_i$  with respect to the undeformed element size  $h_{el}$  for  $c = \{0, 0.15, 0.3\}$  from left to right.  $\square$  :  $N = 2$ ,  $\circ$  :  $N = 5$ ,  $\nabla$  :  $N = 10$ .  $\|z\|_\infty$  from (46) with  $z_i = \mathbf{u}_m^h(x_{1,i}, x_{2,i}) - \mathbf{u}_m^{ex}(x_{1,i}, x_{2,i})$ , where  $\mathbf{u}_m^h$  is defined in (34), and  $(x_{1,i}, x_{2,i})$  are the coordinates of an amount of preselected points.

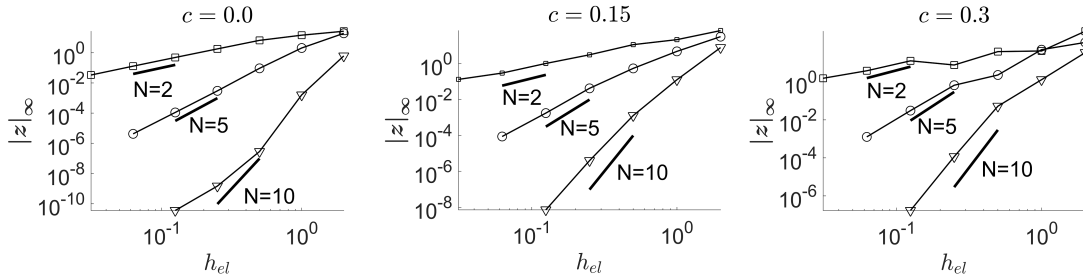


Figure 10. Convergence for  $\sigma_{mm}$  with respect to the undeformed element size  $h_{el}$  for  $c = \{0, 0.15, 0.3\}$  from left to right.  $\square$  :  $N = 2$ ,  $\circ$  :  $N = 5$ ,  $\nabla$  :  $N = 10$ .  $\|z\|_\infty$  from (46) with  $z_i = \sigma_{mm}^h(x_{1,i}, x_{2,i}) - \sigma_{mm}^{ex}(x_{1,i}, x_{2,i})$ , where  $\sigma_{mm}^h$  is defined in (38)-(40), and  $(x_{1,i}, x_{2,i})$  are the coordinates of an amount of preselected points.

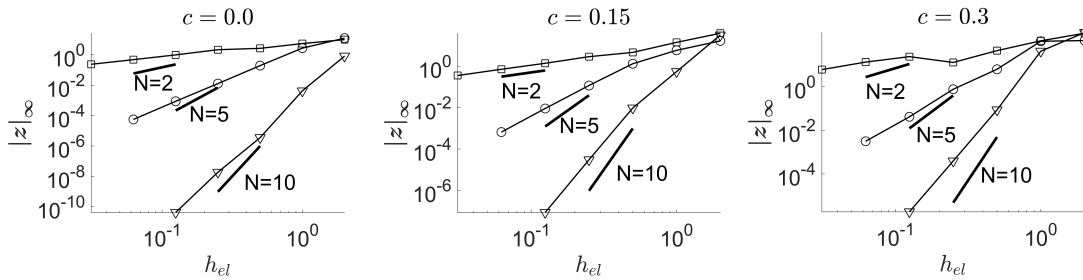


Figure 11. Convergence for  $\sigma_{mn}$  ( $m \neq n$ ) with respect to the undeformed element size  $h_{el}$  for  $c = \{0, 0.15, 0.3\}$  from left to right.  $\square$  :  $N = 2$ ,  $\circ$  :  $N = 5$ ,  $\nabla$  :  $N = 10$ .  $\|z\|_\infty$  from (46) with  $z_i = \sigma_{mn}^h(x_{1,i}, x_{2,i}) - \sigma_{mn}^{ex}(x_{1,i}, x_{2,i})$  for  $m \neq n$ , where  $\sigma_{mn}^h$  is defined in (38)-(40), and  $(x_{1,i}, x_{2,i})$  are the coordinates of an amount of preselected points.

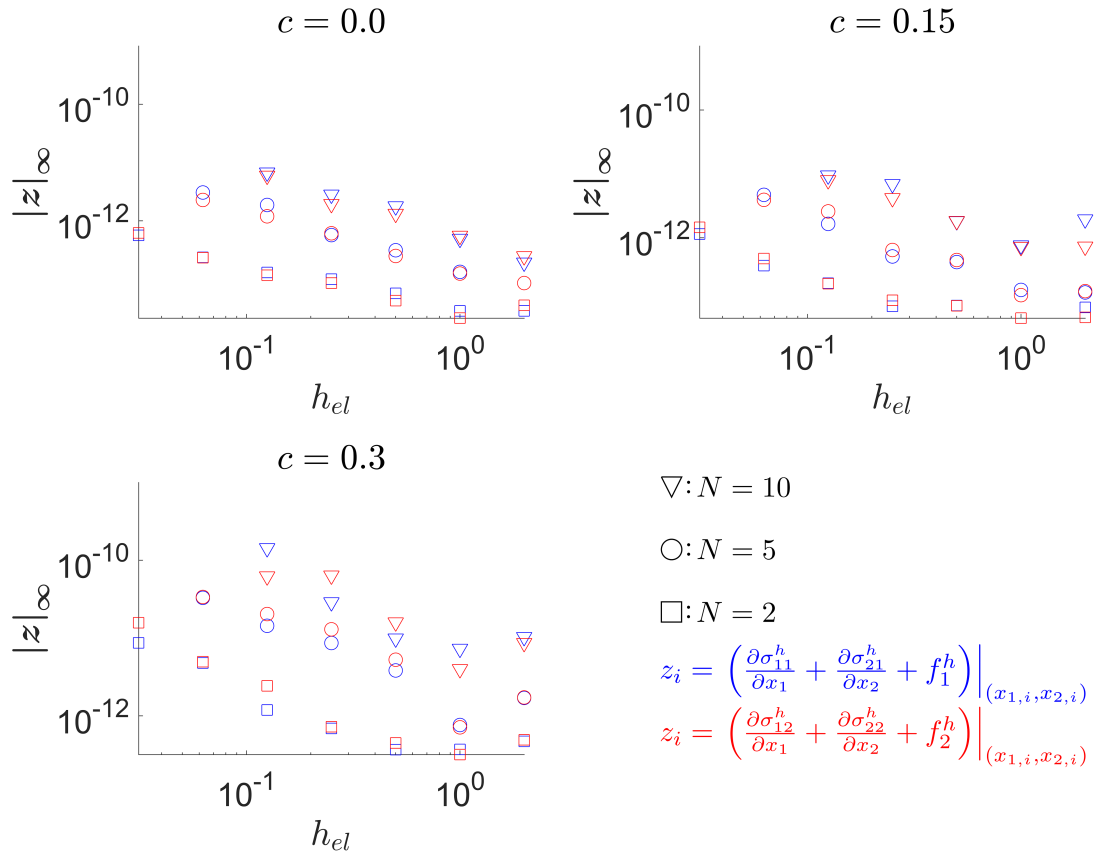


Figure 12. The residual of the force equilibrium equations with respect to the undeformed element size  $h_{el}$  for  $c = \{0, 0.15, 0.3\}$ .  $\square : N = 2$ ,  $\circ : N = 5$ ,  $\nabla : N = 10$ . The infinity norms is defined in (46).  $(x_{1,i}, x_{2,i})$  are the coordinates of an amount of preselected points.

shear stress field is presented in Figure 11. For a problem with smooth solution with polynomial degree  $P$  we expect a convergence rate of  $\mathcal{O}(h^{P+1})$  [29]. Choosing  $N$  to be the polynomial degree of the GLL Lagrange polynomials then it is seen that the highest polynomial order in (34), (38), (39) and (40) is  $N - 1$ , and therefore the expected convergence rate for displacements and stresses are of  $\mathcal{O}(h^N)$ . So the expected slopes in the plots are 2, 5 and 10, which are drawn as a reference. In general all the expanded variables show optimal convergence rates. The precision is affected by the deformation, but there is still monotonic convergence even for the highly deformed mesh ( $c = 0.3$ ). More interesting is the plot of the residual of the force equilibrium equations in Figure 12, which are calculated as

$$R_{fe}(x(\xi)) = \left( \sum_{s=1}^{N_s} \left( \mathcal{I}^{(3)}(x(\xi)) \right) \mathcal{D} \Delta_{\hat{T}} + \sum_{s=1}^{N_s} \left( \mathcal{I}^{(3)}(x(\xi)) \right) \mathbf{F} \right) \frac{1}{J(x(\xi))},$$

where  $J(x(\xi))$  is the determinant of the Jacobian matrix, and  $\mathcal{I}^{(3)}$  is defined in (42).

The plots show that the force equilibrium equations are satisfied to machine precision independent of the resolution of the computational domain. This means that the numerical errors are confined to the constitutive equations. In fact even when the grid are overlapping for  $c = 0.6$  in Figure 13 the solution still converges. Here the number of elements are  $2 \times 2$  with polynomial degree  $N = 30$ , which produces the errors listed in Table I. The residual of the force equilibrium equations evaluated over the domain is plotted in Figure 14, and as seen the residual is of order  $10^{-11}$ .

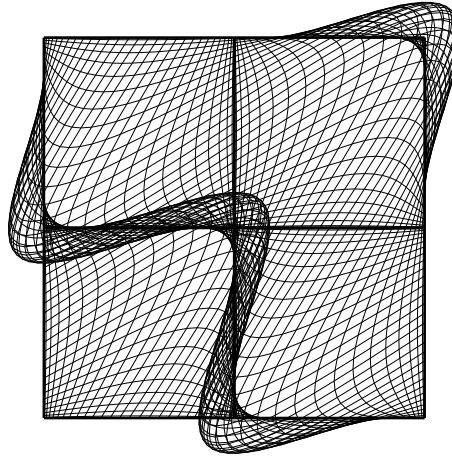


Figure 13. Deformed grid for  $2 \times 2$  elements with polynomial degree  $N = 30$  and  $c = 0.6$ .

Table I. Values of  $|z|_\infty$  in (46) for the displacement and stress fields in the test case of the deformed grid in Figure 13, and  $(x_{1,i}, x_{2,i})$  are the coordinates of an amount of preselected points.

$z_i$	$ z _\infty$
$u_m^h(x_{1,i}, x_{2,i}) - u_m^{ex}(x_{1,i}, x_{2,i})$	0.0026
$\sigma_{mm}^h(x_{1,i}, x_{2,i}) - \sigma_{mm}^{ex}(x_{1,i}, x_{2,i})$	0.0353
$\sigma_{mn}^h(x_{1,i}, x_{2,i}) - \sigma_{mn}^{ex}(x_{1,i}, x_{2,i})$ ( $m \neq n$ )	0.0464

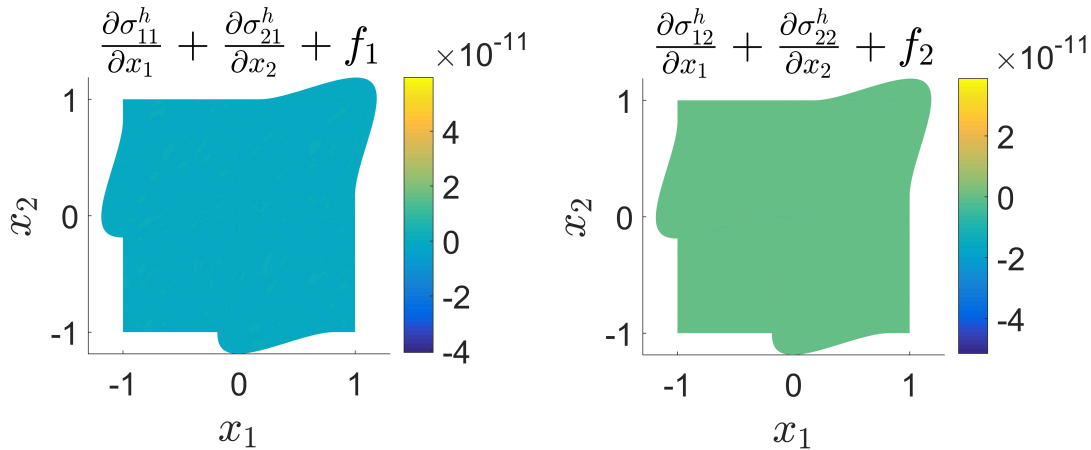


Figure 14. The residual of the force equilibrium equations in the domain for the grid in Figure 13.

## 7.2. Plate with Circular Hole

The last test case is for the stress concentration of a circular hole in the plate shown in Figure 15, which has a uni-directional loading. The exact solution for a circular hole in an infinite large plate is given in many textbooks on stress analysis, e.g. [30, p. 306]. By using symmetry conditions only a quarter of the domain is considered. The boundary condition and the grid resolution are shown on Figure 15. The elements are mapped to the reference domain with a transfinite map. The solution of the displacement field stress field and the residual of the force equilibrium equations are plotted in Figure 16, and the residual of the force equilibrium equations are of order  $10^{-13}$ . The largest errors in the domain are listed in Table II. As seen from the norms the solution of  $\sigma_{12}^h$  and  $\sigma_{21}^h$  are not

Table II. Values of  $|z|_\infty$  in (46) for the displacement and stress fields in the test case of the circular hole in Figure 15, and  $(x_{1,i}, x_{2,i})$  are the coordinates of an amount of preselected points.

$z_i$	$ z _\infty$
$u_1^h(x_{1,i}, x_{2,i}) - u_1^{ex}(x_{1,i}, x_{2,i})$	$5.3869 \cdot 10^{-7}$
$u_2^h(x_{1,i}, x_{2,i}) - u_2^{ex}(x_{1,i}, x_{2,i})$	$5.7281 \cdot 10^{-7}$
$\sigma_{11}^h(x_{1,i}, x_{2,i}) - \sigma_{11}^{ex}(x_{1,i}, x_{2,i})$	$2.7830 \cdot 10^{-5}$
$\sigma_{21}^h(x_{1,i}, x_{2,i}) - \sigma_{21}^{ex}(x_{1,i}, x_{2,i})$	$2.9794 \cdot 10^{-5}$
$\sigma_{12}^h(x_{1,i}, x_{2,i}) - \sigma_{12}^{ex}(x_{1,i}, x_{2,i})$	$2.8683 \cdot 10^{-5}$
$\sigma_{22}^h(x_{1,i}, x_{2,i}) - \sigma_{22}^{ex}(x_{1,i}, x_{2,i})$	$2.6685 \cdot 10^{-5}$

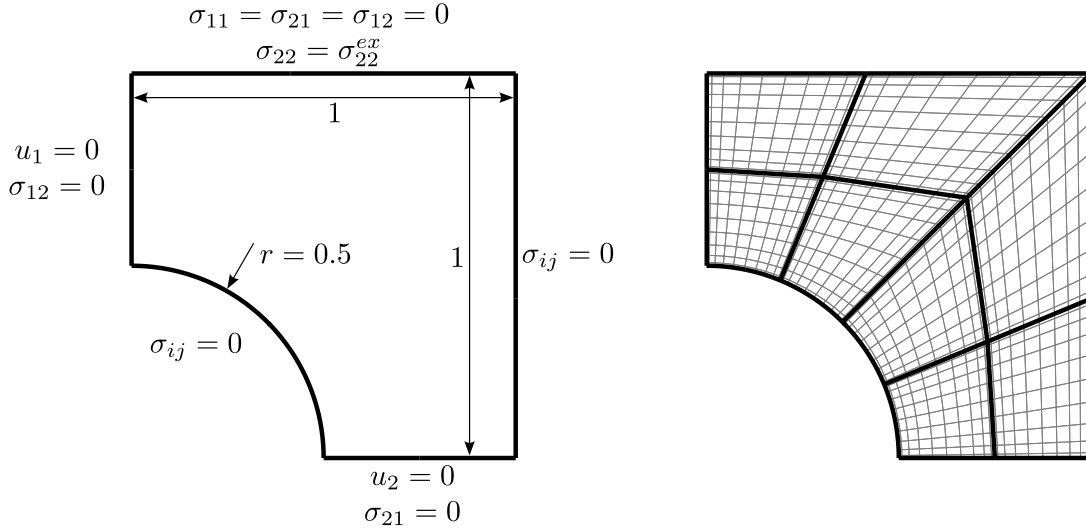


Figure 15. The quarter section of a circular hole of size  $r = 0.5$  in a plate of size  $2 \times 2$ . Left: The boundary conditions. Right: The grid consisting of 8 spectral elements with polynomials degree  $N = 10$ .

equal, which is expected as they are expanded by different polynomial see (38) and (39). They are, however, very close.

## 8. CONCLUSION

In this paper a spectral element method is presented, which satisfies the equilibrium of forces in a structural problem to machine precision, independent of the size and shape of the individual elements. The convergence rate of the problem is completely determined based on the order of the polynomial expansions. The method incorporates the geometry and the governing equations in the discrete problem, and through the *edge expansion polynomials* unknowns associated to lines, surfaces, and volume are expanded. Surface forces are expanded as surface values and are continuous between elements boundaries meaning that Newton's third law is satisfied between elements. This fact also makes the method very robust and produces convergent solutions for even highly deformed elements.

## REFERENCES

1. Zienkiewicz OC. *The Finite Element Method in Engineering Science*. McGraw-Hill Inc. 1972.
2. Oden JT, Reddy JN. *Mathematical Theory of Finite Elements*. John Wiley and sons. 1976.
3. Bathe KJ, Wilson EL. *Numerical Methods in Finite Element Analysis*. Prentice-Hall. 1976.
4. Reddy JN. *An Introduction to the Finite Element Method* (3rd edn). McGraw-Hill. 2006.
5. Reddy JN, Gartling DK. *The Finite Element Method in Heat Transfer and Fluid Dynamics*. CRC Press. 1997.

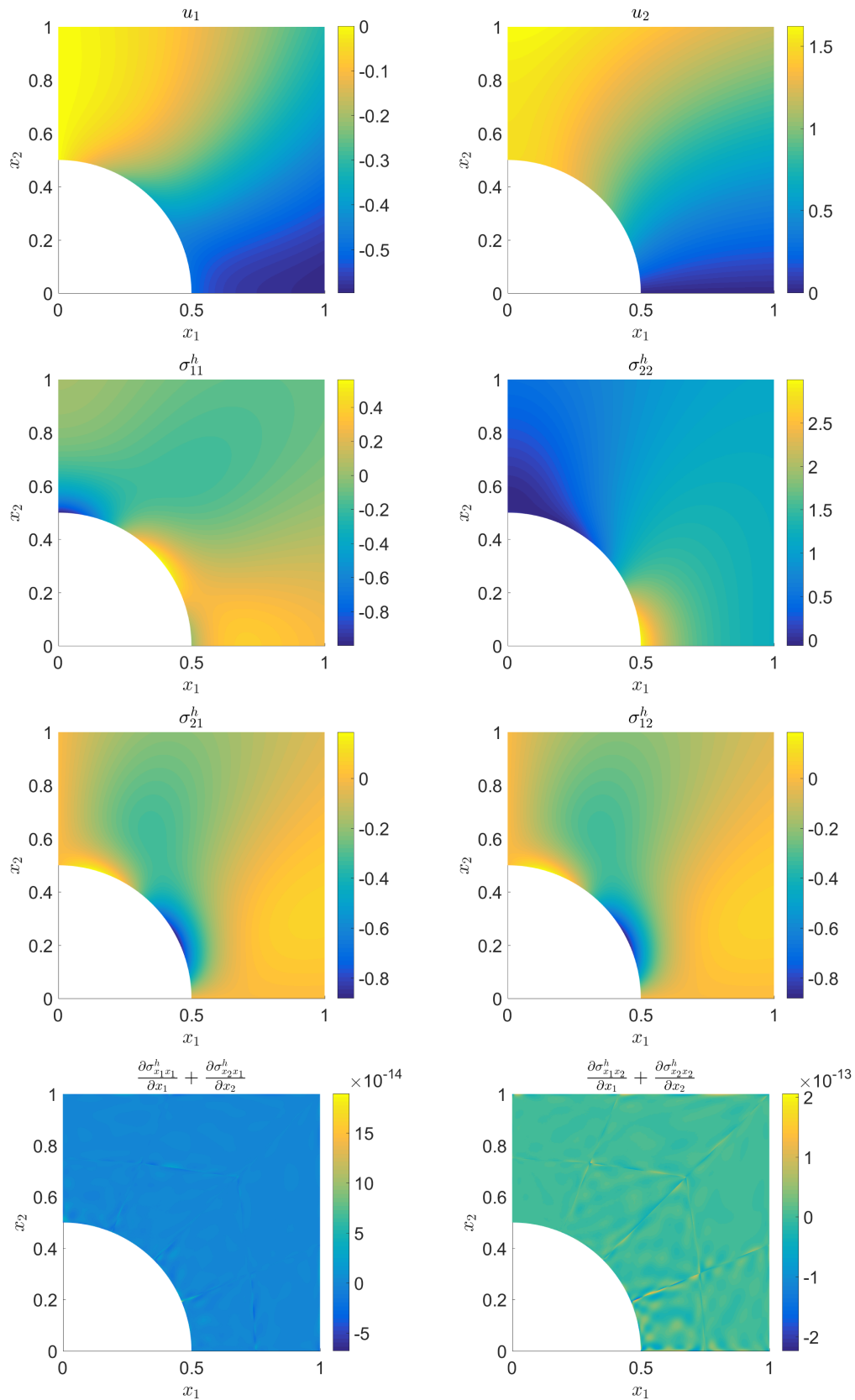


Figure 16. The solution of the test case in Figure 15 as well as the residual of the force equilibrium equations.

6. Monk P. *Finite Element Methods for Maxwell's Equations*. Oxford Science Publications. 2003.
7. Cook RD, Malkus DS, Plesha ME, Witt RJ. *Concepts and Applications of Finite Element Analysis* (4th edn). John Wiley and sons. 2001.
8. Marsden JE, Hughes TJR. *Mathematical Foundations of Elasticity*. Prentice-Hall,. 1983.
9. Bochev S P, Hyman J. Principles of Mimetic Discretizations of Differential Operators. *Compatible Spatial Discretizations*, Eds.: D. Arnold, P. Bochev, R. Nicolaides and M. Shashkov, *The IMA volumes in Mathematics and its Applications* 2006; **142**:89–119.
10. Bonelle J, Ern A. Analysis of Compatible Discrete Operator Schemes for Elliptic Problems on Polyhedral Meshes. *ESAIM Mathematical Modelling and Numerical Analysis* 2014; **48**(2):553–581.
11. Tonti E. Why Starting from Differential Equations for Computational Physics?. *Journal of Computational Physics* 2014; **257**:1260–1290.
12. Kreeft J, Palha A, Gerritsma M. Mimetic Framework on Curvilinear Quadrilaterals of Arbitrary Order. *Arxiv preprint* 2011.
13. Kreeft J, Gerritsma M. Mixed Mimetic Spectral Element Method for Stokes Flow: A Pointwise Divergence-free Solution. *Journal of Computational Physics* 2013; **240**:284–309.
14. Gerritsma M. Edge Functions for Spectral Element Methods. *Spectral and High Order Methods for Partial Differential Equations - Lecture Notes in Computational Science and Engineering* 2010; **76**:199–207.
15. Arnold DN, Falk RS, Winther R. Differential Complexes and Stability of Finite Element Methods II: The Elasticity Complex. *Compatible Spatial Discretizations*, Eds.: D. Arnold, P. Bochev, R. Nicolaides and M. Shashkov, *The IMA volumes in Mathematics and its Applications* 2006; **142**:47–67.
16. Yavari A. On Geometric Discretization of Elasticity. *Journal of Mathematical Physics* 2008; **49**.
17. Angoshtari A, Yavari A. A Geometric Structure-preserving Discretization Scheme for Incompressible Linearized Elasticity. *Computer Methods in Applied Mechanics and Engineering* 2013; **259**:130–153.
18. Yavari A, Goriely A. Nonlinear Elastic Inclusions in Isotropic Solids. *Proceedings of the Royal Society A* 2013; **469**.
19. Angoshtari A, Yavari A. Differential Complexes in Continuum Mechanics. *Archive for Rational Mechanics and Analysis* 2014; **216**:193–220.
20. Reddy JN, Srinivasa A. On the Force-Displacement Characteristics of Finite Elements for Elasticity and Related Problems. *Finite Elements in Analysis and Design* 2015; **104**:35–40.
21. Hughes TJR. *The Finite Element Method: Linear Static and Dynamic Finite Element Analysis*. Prentice-Hall. 1987.
22. Timoshenko SP, Goodier JN. *Theory of Elasticity*. (3rd edn, International student edn). McGraw-Hill. 1982.
23. Gerritsma M. An Introduction to a Compatible Spectral Discretization Method. *Mechanics of Advanced Materials and Structures* 2012; **19**(1-3):48–67.
24. Kreyszig E. *Advanced Engineering Mathematics* (9th edn). John Wiley and Sons. 2005.
25. Kanso E, Arroyo M, Tong Y, Yavari A, Marsden JE, Desbrun M. On the Geometric Character of Stress in Continuum Mechanics. *Zeitschrift für angewandte Mathematik und Physik* 2007; **58**:843–856.
26. Tarhasaari T, Kettunen L, Bossavit A. Some Realizations of a Discrete Hodge Operator: A Reinterpretation of Finite Element Techniques. *IEEE Transactions on Magnetics* 1999; **35**(3):1494–1497.
27. Lipnikova K, Manzinia G, Shashkov M. Mimetic Finite Difference Method. *Journal of Computational Physics* 2014; **257**:1163–1227.
28. Canuto C, Hussaini M, Quarteroni A, Zang T. *Spectral Methods, Fundamentals in Single Domains* Springer. 2006.
29. Karniadakis GE, Spencer SJ. *Spectral/hp Element Methods for Computational Fluid Dynamics* (2nd edn). Oxford Science Publications. 2005.
30. Reddy JN. *An Introduction to Continuum Mechanics* (2nd edn). Cambridge University Press. 2013.